IS-4711
UC 90

MASTER

FOSSIL ENERGY PROGRAM

Technical Progress Report

1 April 1979 through 30 June 1979

I. Mining Research and Development - Coal Preparation and Analysis

II. Advanced Research and Technology Development

AMES LABORATORY

Iowa State University

Ames, Iowa 50011

Date Transmitted: September 1979

Prepared for the U. S. Department of Energy
Under Contract No. W-7405-eng-82

NOTICE

Available from: National Technical Information Service
U. S. Department of Commerce
P.O. Box 1553
Springfield, VA 22161

Price: Microfiche $3.00
Printed Copy

Table of Contents

Abstract

This report covers objectives and progress for areas of the Ames Laboratory Fossil Energy Program. The period covered is 1 April 1979 through 30 June 1979.

A. MICROSTRUCTURE OF COAL

Raymond T. Greer

Abstract:

In alkaline leaching of pyrite and of pyrite in coal, the major reaction product in desulfurization under specific conditions is hematite. In addition, direct evidence is presented for microstructural differences among concentric bands in hematite reaction rims surrounding unreacted pyrite. Hematite rims are found to contain a small amount of sulfur.

In applying a new direct method for the determination of organic sulfur in coal macerals, iron and calcium are also monitored. This has provided the unexpected information that the alkaline leaching treatment results in a substantial calcium buildup in vitrinite (for both a one-step and a two-step method of desulfurization described in the preceding report).

Objectives and Scope of Work:

Background - - In the desulfurization of pyrite, microstructural and chemical changes are described and identified to contribute information toward process development. Organic sulfur distribution and concentration differences within and among coal macerals are being characterized. The purpose of this work is to establish how desulfurization techniques affect removal of organic sulfur and other forms of sulfur, and to directly quantify changes.

STATUS

I. Chemical Desulfurization

Chemical Leaching of Pyrite - - Fine-size pyrite particles leached with a hot, dilute solution of sodium carbonate containing dissolved oxygen under pressure

are being studied to monitor the nature and extent of phase transformation products in desulfurization experiments. The primary fine grained reaction product has been identified as hematite, Fe_2O_3 [Ref. 1]. In addition, an important direct observation of concentric bands of different microstructure in the hematite reaction rim has been made. Examples follow.

Reaction conditions for samples from a tubular bed reactor system are listed in Table 1. These samples are arranged in a similar way for the "sample collected" columns of Table 1 and the reflected light polished section viewed of reacted pyrite in Figure 1. Control pyrite sections are shown in Figure 2 (samples S135 and S136 of Table 1). These are representative particle views. With higher oxygen partial pressures, more material is transformed. Another trend suggested by the micrographs of Figure 1 is that for the tubular bed reactor samples, the reacted material (or rim) appears thicker on one side than another. In Figure 1, the bright central regions are pyrite (P). The reacted material (dark gray) is indicated by arrows.

In Table 2, conditions for leached pyrite specimens from a stirred autoclave system are listed. The associated reflected light microscopy sections are shown in Figure 3 for a control and for reacted samples. Again, the central bright areas are pyrite (P), and the reacted material is shown by arrows. Compare the relative uniformity of the reaction rims in Figure 3 with those in Figure 1.

Closer examination of Figure 1 and 3 reveals a dark gray thin rim surrounding unreacted pyrite (e.g. S-128, S-134, or PYB-100) and a lighter gray thicker concentric outer rim of reaction product. This is more easily seen in the colors of reflected light (selected color photos are available on request). This is shown schematically in Figure 4.

Table 1. Leaching of Pyrite - Tubular Reactor System.

Run Number	Pyrite	Up Stream Pressure	Temperature	Reagent	Reagent Flow Rate	O_2 Flow Rate	Reaction Time	Sample Collected*		
								Front	Middle	Rear
70	unwashed -40/+60 mesh	150 psig	150°C	2 wt.% Na_2CO_3	1.5ml/sec	9.5ml/sec	1 hr.	S123	S124	S125
71	unwashed -40/+60 mesh	400 psig	150°C	2 wt.% Na_2CO_3	1.5ml/sec	9.5ml/sec	1 hr.	S126	S127	S128
72	washed** -40/+60 mesh	400 psig	150°C	2 wt.% Na_2CO_3	1.5ml/sec	9.5ml/sec	1 hr.	S129	S130	S131
73	washed** -40/+60 mesh	150 psig	150°C	2 wt.% Na_2CO_3	1.5ml/sec	9.5ml/sec	1 hr.	S132	S133	S134
S135	Control -40/+60 mesh unwashed	--	--	--	--	--	--	--	--	--
S136	Control -40/+60 mesh washed**	--	--	--	--	--	--	--	--	--

*schematic:

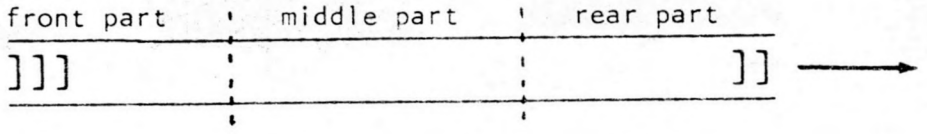

**washed samples: 70°C, 1 hr., in 10% HCl - 90% distilled water ... to remove soluble sulfates

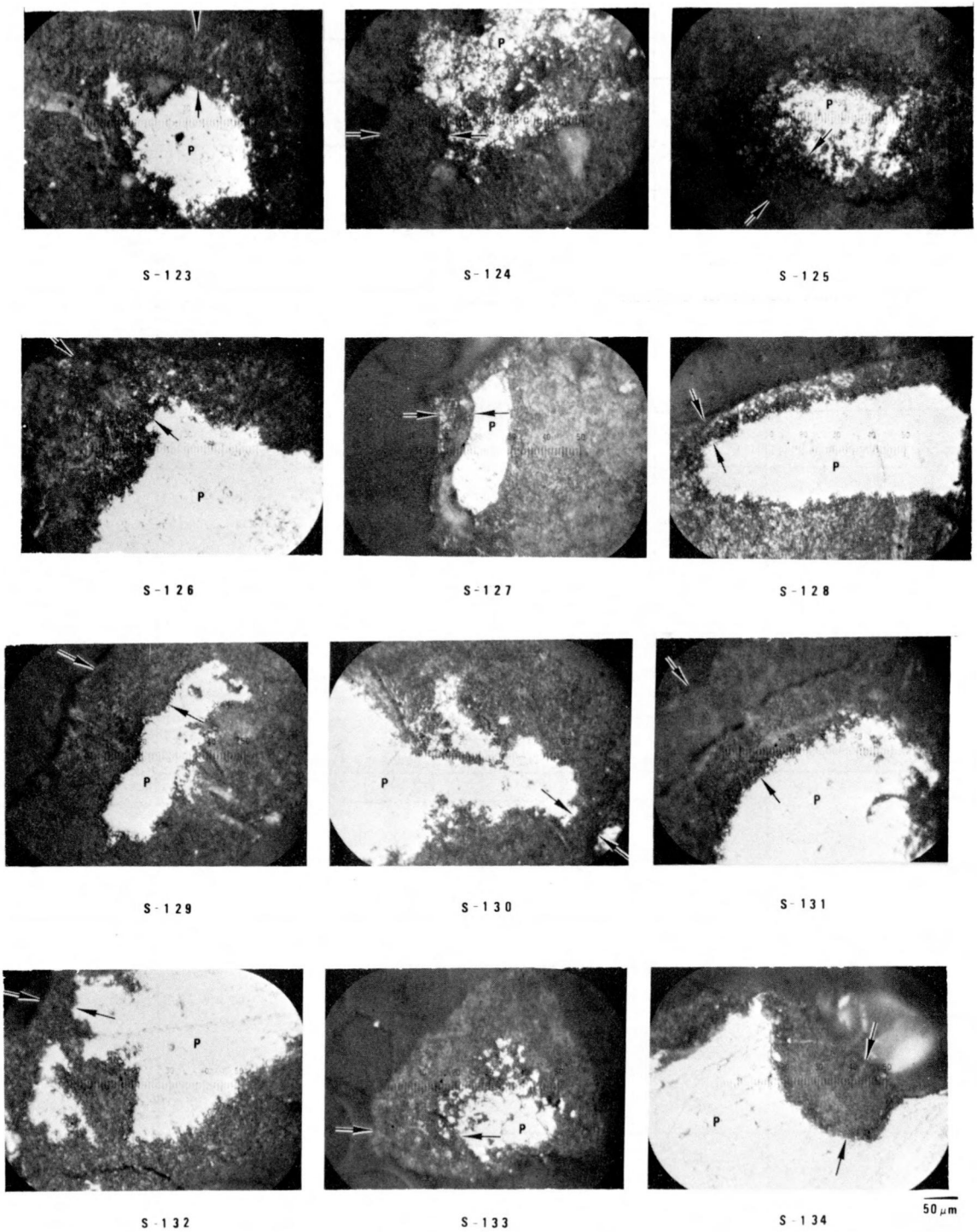

Figure 1. Reflected light microscopy images of polished sections of partially reacted pyrite from chemical leaching treatment in a tubular bed reactor system. Bright central areas (P) are unreacted pyrite. Arrows delineate reaction product rim.

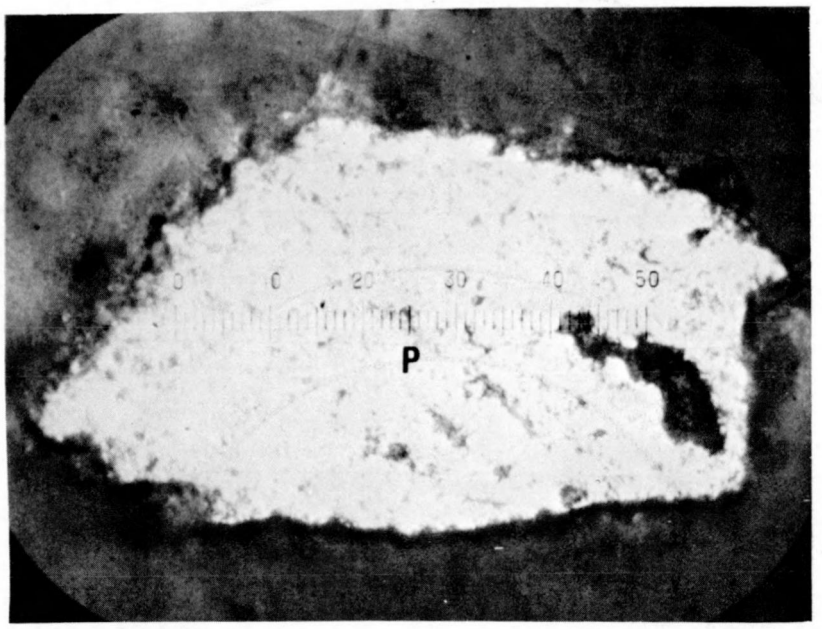

S - 1 35

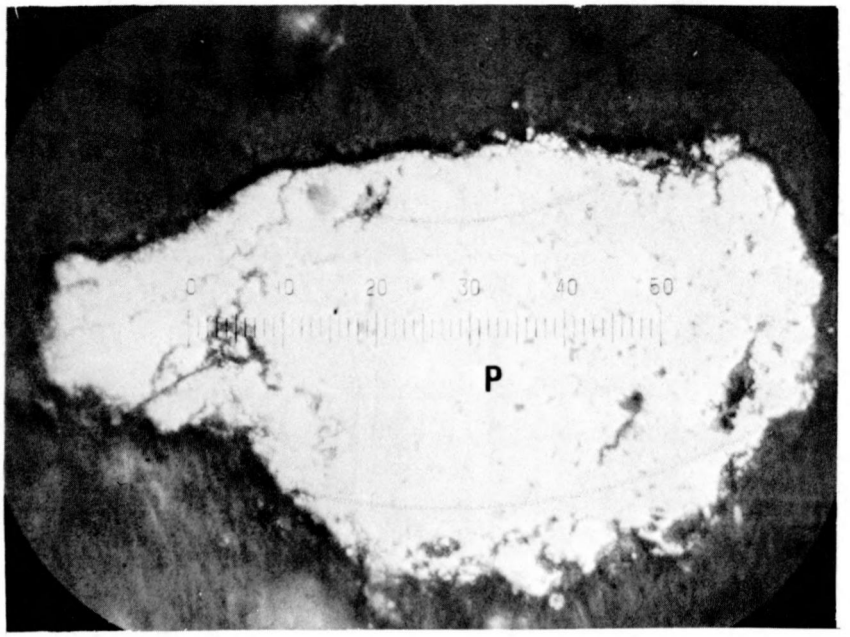

S - 1 3 6

50 μm

Figure 2. Reflected light microscopy images of polished sections of control pyrite (P) sections. Compare with sections in Figure 1.

Table 2. Leaching of Pyrite: Stirred Autoclave System.

Number	Mesh	Treatment	Na_2CO_3 M	X-ray**
PYB68	-60/100	cleaned pyrite* 150°C, 1 hr., p.p. O_2=200psia	0.2	hematite + trace maghemite
PYB74	-140/170	cleaned pyrite 150°C, 1 hr., p.p. O_2=200psia	0.2	hematite + trace maghemite
PYB100	-60/100	cleaned pyrite 150°C, 1 hr., p.p. O_2=25psia	0.2	hematite + trace maghemite
PYB101	-230	cleaned pyrite 150°C, 1 hr., p.p. O_2=50psia	0.2	hematite + trace maghemite
PYB102	-230	cleaned pyrite 150°C, 1 hr., p.p. O_2=155psia	0.0 (use distilled water)	hematite + trace maghemite
PYB37	-170/200	cleaned pyrite, control	--	pyrite

*HCl cleaned (10% conc. HCl, 90% H_2O)

**Unreacted pyrite is also present in each case.

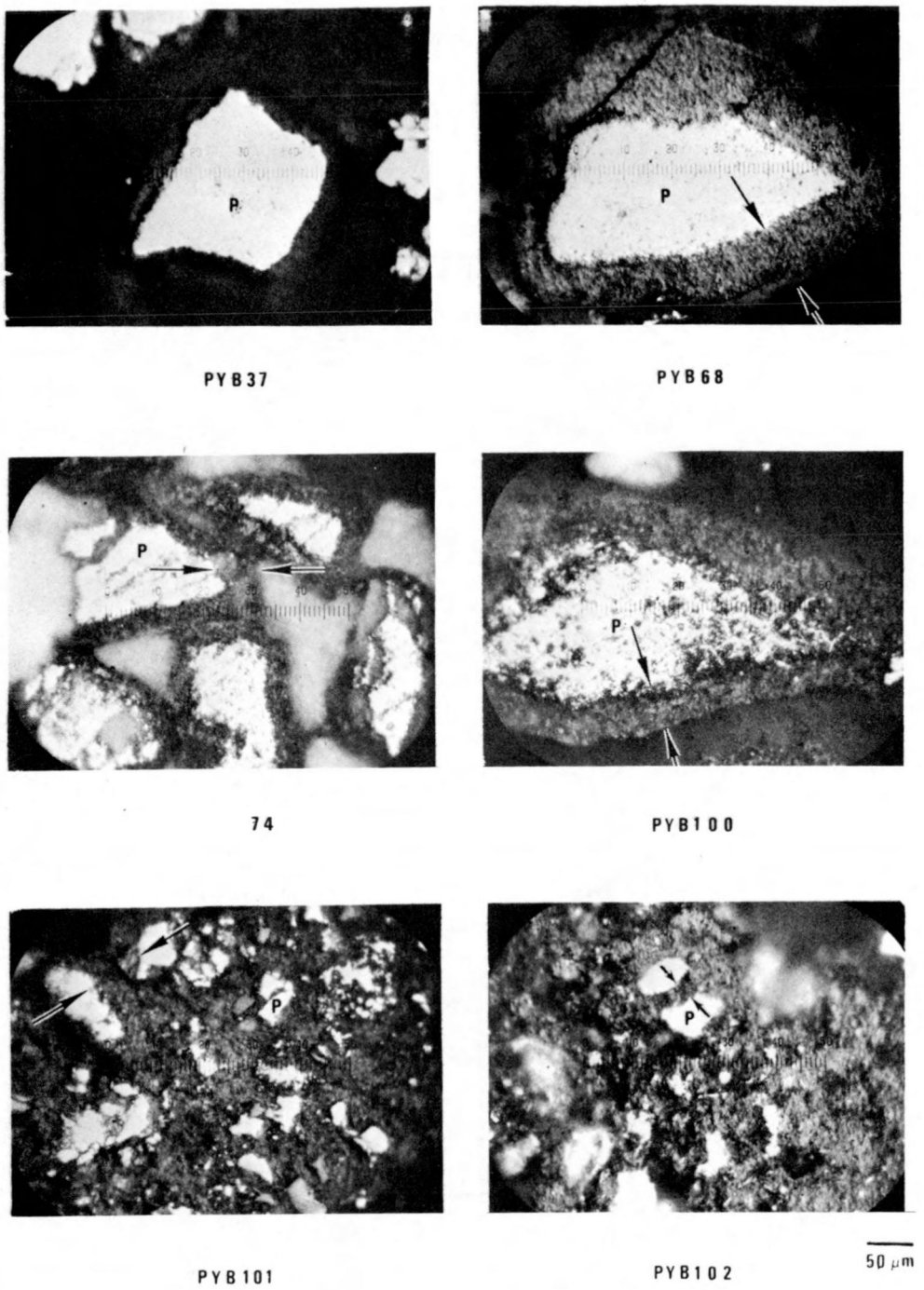

Figure 3. Reflected light microscopy images of polished sections of partially reacted pyrite from chemical leaching treatment in a stirred autoclave system. Bright central areas (P) are unreacted pyrite. Arrows delineate reaction product rim. PYB37 is a pyrite control.

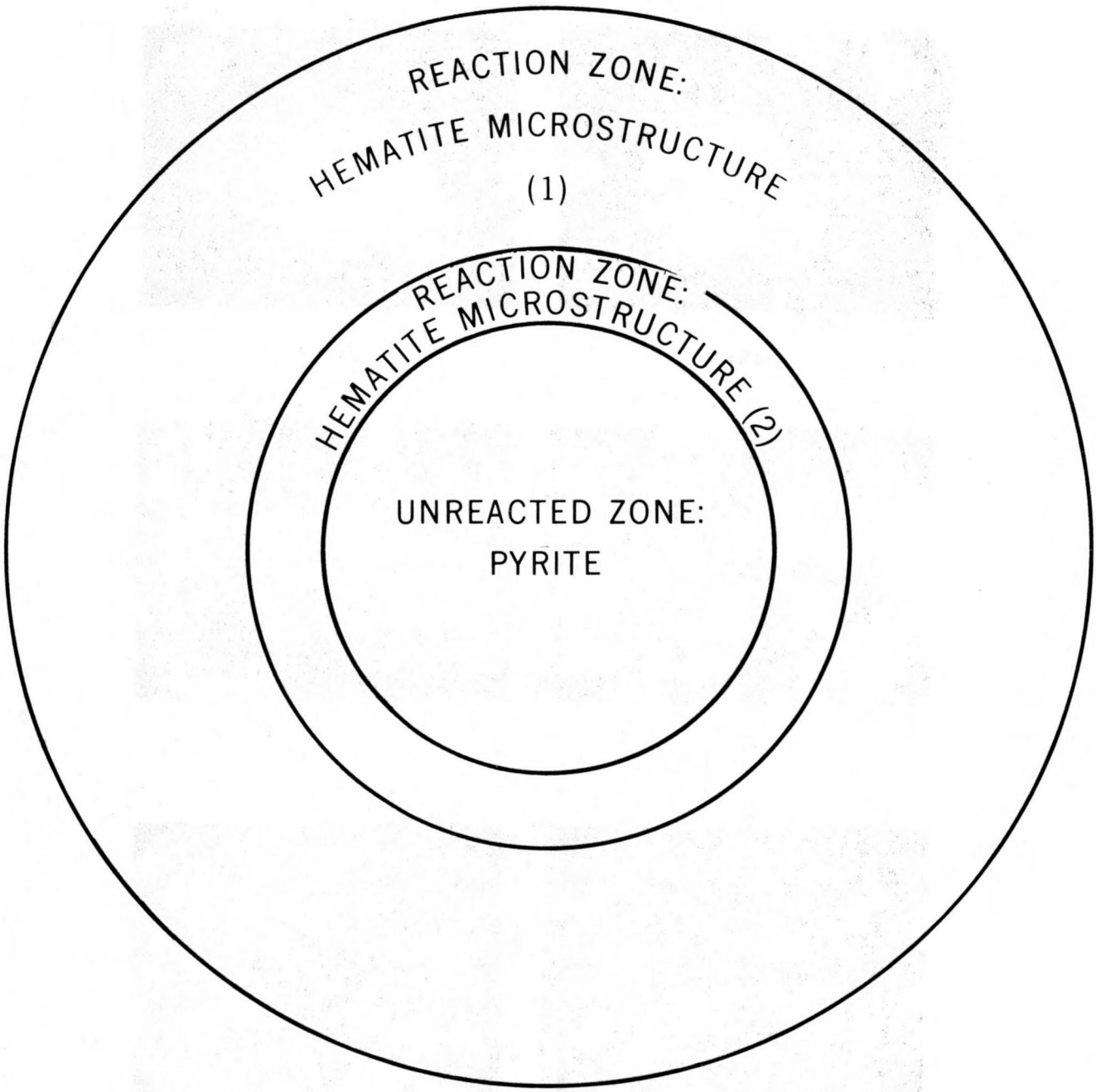

Figure 4. Schematic of partially reacted pyrite from chemical leaching treatment. A thin reaction zone contacting unreacted pyrite (FeS_2) exhibits a somewhat different microstructure than the outer reaction zone. The major rim reaction product is hematite (Fe_2O_3).

Two aspects are initially of interest: porosity variations among the zones and/or phase changes. In Figure 5, a secondary electron image (obtained by using a scanning electron microscope) is shown. Compare this image with the sulfur elemental image. A small amount of sulfur is detected in the Fe_2O_3 exterior reaction rim, whereas the sulfur in the pyrite region is relatively high. The sulfur elemental scan shows that phase changes occur. Additional examples are shown in Figure 6 (tubular bed reactor sample; mirror image of S-134 of Figure 1). The higher magnification view in Figure 6 shows we have major porosity changes among the three general regions (two concentric hematite regions varying in microstructure, and pyrite). Even for these polished surfaces (compared with fracture surfaces), it is apparent that each region is different in its general structural character. In a practical sense, this may significantly influence the effectiveness of the conversion of pyrite to hematite.

Additional samples of leached pyrite have been provided by T. Wheelock and co-workers. These have been selected from a series that represents changes in the extent of conversion of pyrite to hematite with increasing times in an autoclave reaction system. These samples are being investigated to possibly reveal information which might explain why less reaction product was formed at the longer reaction times than was predicted. Sections through representative particles from five cases listed in Table 3 are shown in Figure 7. X-ray diffraction indicates that hematite is the primary reaction product in each case. Reflected light observations (Figure 7) reveal that the major material in the reaction rim is hematite, and that a small reaction zone between the hematite and the unreacted pyrite may be present (possibly due to microstructural differences similar to the example shown for the tubular bed reactor

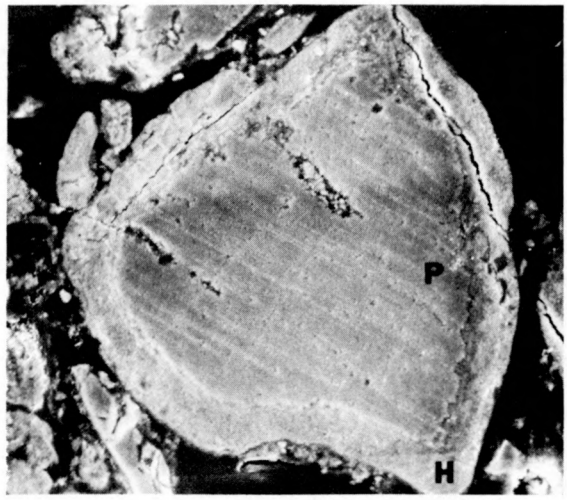

PYB-68
SECONDARY ELECTRON IMAGE

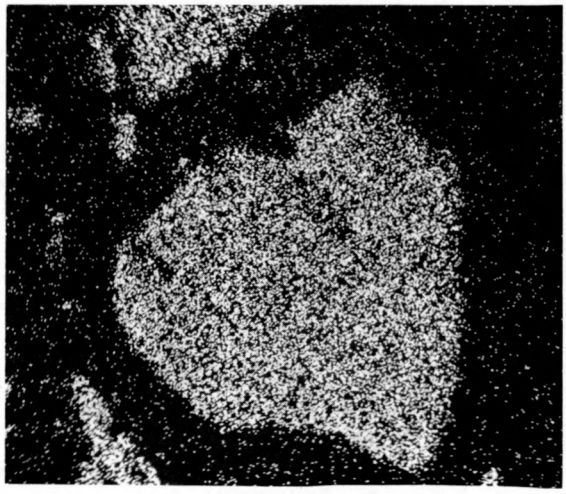

PYB-68
SULFUR IMAGE

25 μm

Figure 5. The large leached particle (autoclave reaction system) filling most of the field of view of the secondary electron image is primarily unreacted pyrite (P, central portion of micrograph). The reaction rim is predominantly hematite (H). The sulfur image shows 1) a small amount of sulfur in the hematite (H) concentric zone, and 2) the relatively high sulfur content in the central portion (i.e., the unreacted pyrite). The sulfur image can be compared directly with the secondary electron image.

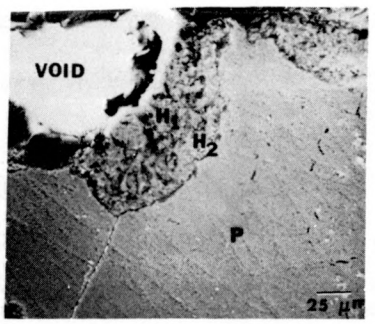

S-134
SECONDARY ELECTRON IMAGE

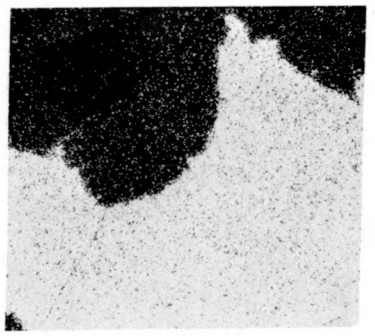

S-134
SULFUR IMAGE 25 μm

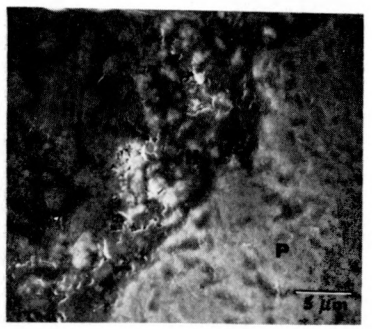

S-134
HIGHER MAGNIFICATION SECONDARY ELECTRON IMAGE

Figure 6. The leached pyrite (tubular bed reactor system) comprizing the secondary electron image is a mirror image of S-134 in Figure 3. Major phases are hematite (H) and pyrite (P). Compare the sulfur and the secondary electron image (same magnification). The higher magnification view of the center of the top micrograph of the figure includes the three major microstructural features: upper left region is hematite (H_1), central band from upper right to lower left is also hematite (H_2), and lower right region is pyrite. The microstructure in each zone is distinct and different among the three.

Table 3. Leaching of Pyrite: Stirred Autoclave System; Pyrite Conversion.

Sample Number	Mesh	Treatment	Na_2CO_3 M	Sulfur Conversion,** wt.%
PA08-[1]	-40/60	cleaned pyrite*, 150°C, 1200 sec reaction time, p.p.O_2 = 50 psia	0.2	24.38
PA08-[2]	-40/60	cleaned pyrite, 150°C, 2400 sec. reaction time, p.p.O_2 = 50 psia	0.2	35.66
PA08-1-[3]	-40/60	cleaned pyrite, 150°C, 3600 sec. reaction time, p.p.O_2 = 50 psia	0.2	38.59
PA08-2-[4]	-40/60	cleaned pyrite, 150°C, 2 hours reaction time, p.p.O_2 = 50 psia	0.2	49.41
PA08-2-[5]	-40/60	cleaned pyrite, 150°C, 3 hours reaction time, p.p.O_2 = 50 psia	0.2	49.56

*HCl cleaned (10% conc. HCl, 90% H_2O)

**Sulfur removed compared with total sulfur originally in sample.

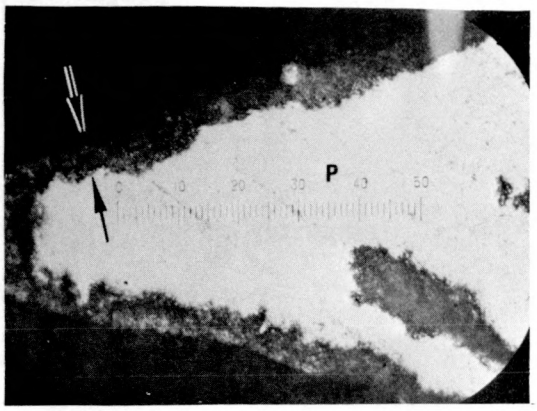

PA08-[1]

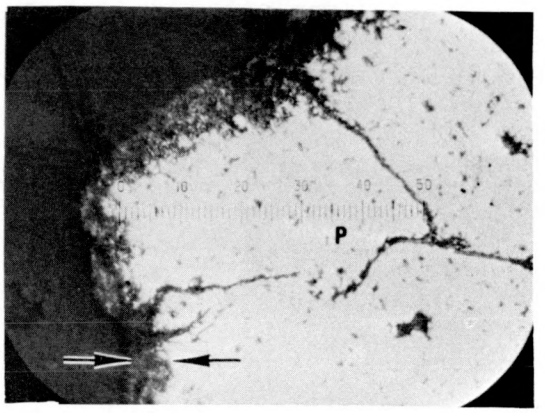

PA08-1-[2]

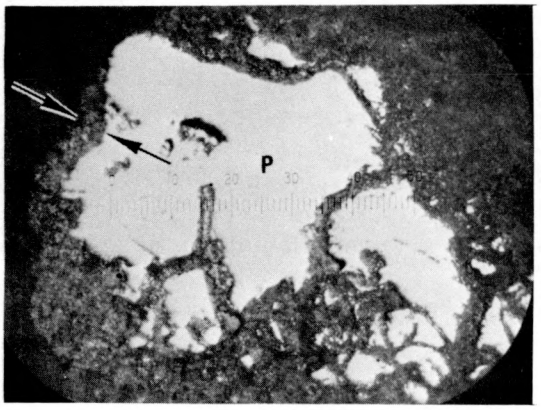

PA08-1-[3]

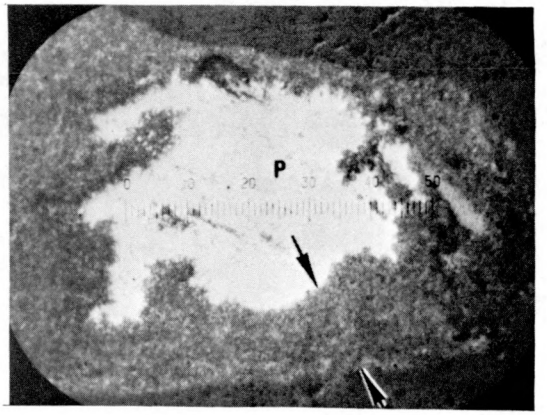

PA08-2-[4]

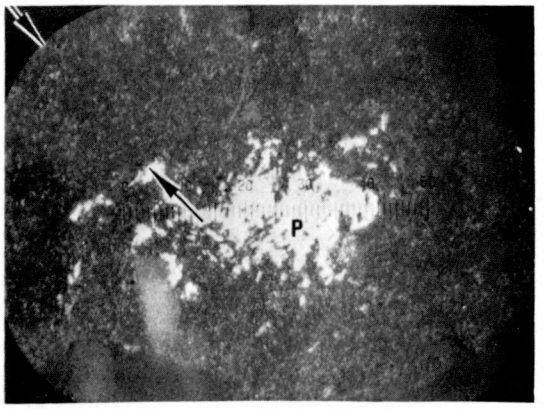

50 μm

PA08-2-[5]

Figure 7. Sections of leached pyrite grains (stirred autoclave system) representing increasing residence times in the reactor (from PA08- 1 through PA08-2- 5).

system (Figure 6). Energy dispersive elemental X-ray analytical studies and scanning electron microscope textural studies to confirm the presence and nature of this second zone are in progress.

Chemical Leaching of Coals

1. Pyrite Conversion - - Reflected light microscopy of polished sections through the coals of Table 1 in reference 1 and Table 2 of reference 2 indicate a thin dark band between the unreacted pyrite in a coal and hematite (red in reflected light) reaction product. Detailed combined analytical studies using energy dispersive X-ray analysis (for elemental distribution work) and scanning electron microscopy (Microtextural differences) are in progress.

2. Calcium Buildup in Vitrinite - - In the process of investigating the presence, amounts and distribution of organic sulfur in both control and desulfurized coals (removal of sulfur by leaching with a hot, dilute solution of sodium carbonate containing dissolved oxygen under pressure) an important observation was made concerning the calcium content in vitrinite. The calcium content in the vitrinite of treated coals appears to be significantly higher than in vitrinite of control coals. A possible explanation is that this desulfurization treatment apparently frees calcium to the leach solution from the inorganic calcium-bearing minerals in the coal, and a significant amount of this calcium is subsequently found in the vitrinite of the treated coals of Table 1, Ref. 1. Prior to desulfurization, the calcium content of the vitrinite is generally less than 0.1 weight percent. After desulfurization, the average calcium content appears to be of the order of one to two weight percent.

II. Organic Sulfur

A. Direct Characterization

To study the presence, distribution and amounts of organic sulfur present in leached and in untreated coals, an electron microprobe X-ray analyzer (Applied Research Laboratories) equipped with an energy dispersive X-ray analyzer is used. Currently, crushed coals are being examined (-200/+250 mesh; Table 1 of Ref. 1). Samples are mounted in a conductive mount, are polished, and receive no coatings. Quantitative data are obtained on a point-by-point basis for sulfur, iron and calcium. The analyses are performed at an electron accelerating potential of 10 keV and a beam current of 16 nanoamperes. Curved crystal spectrometers are utilized for elemental determinations. An ammonium dihydrogen phosphate analyzing crystal is used for the sulfur K_α X-ray emission line, and a lithium fluoride analyzing crystal for iron and calcium.

In an analysis, vitrinite grains, for example, are identified, marked, and photographically recorded at 400x using a reflected light microscope. The sample mount is then ready for point-by-point microprobe analysis. A specimen current image is then obtained (generally at either 400x or 800x) which is used in conjunction with X-ray elemental location maps (two-dimensional dot patterns corresponding to elemental distribution patterns). Sulfur, iron, calcium and oxygen patterns are recorded. These are useful in locating and avoiding inorganic mineral matter in the course of the organic sulfur analyses. Also, since the point-by-point analyses simultaneously record quantitative data for sulfur, iron, and calcium, levels can be set for iron and calcium so that a point is rejected if these are too high (possibly due to microcrystalline pyrite, or gypsum, for example). In this way, analyses can be made just for organic sulfur. However, there is one aspect of this analytical problem which must be accounted for. Elemental sulfur and

organic sulfur emissions will be detected at the same wavelength spectrometer setting (λ = 5.371 A). Therefore, a preliminary elemental sulfur analysis (e.g., by gas chromatography; see Ref. 1, p. 7, Table 4 for data for these coals) may be necessary. The elemental sulfur may occur as an oxidation product of pyrite. The wavelength dispersive and energy dispersive X-ray spectrometers are set to function simultaneously. The energy dispersive system permits the investigator to monitor many other cations of possible interest (e.g., Ba ... a possible indicator of the presence of barite, $BaSO_4$). Five consecutive sets of wavelength dispersive analyses (40 second duration each) are performed for each location within a grain. The data are compared with standards, corrected for background, and quantitative data reduction is made using the comprehensive Microprobe Analysis, General Intensities Correction computer program, MAGIC IV.

Examples are shown for comparative purposes in Figures 8 and 9. Figure 8 shows information for a control coal sample, and Figure 9 presents data for a chemically leached coal sample (Western Kentucky coal, Ref. 1, Tables 1 and 4). In these figures, the locations probed on the vitrinite grains are designated in the optical images (12 points in Figure 8 and 9 points in Figure 9). In the complete analysis, additional coal clusters are analyzed in a similar way. The specimen current images are useful for outlining the macerals of interest. These are compared with the X-ray elemental distribution dot patterns such as shown for sulfur and for calcium in Figures 8 and 9.

The leached coals in Table 1 of Ref. 1 indicate a substantial calcium buildup in the vitrinite of the treated coals compared with the associated control coals (both for the one-step and the two-step methods). Compare the calcium elemental scans of Figures 8 and 9. In control samples, the calcium

Table 4. Sulfatic Sulfur Determinations in Selected Coals.

Sample Number	Seam/State	Rank/Province	Sulfatic Sulfur* weight % (DRY)
PSOC-003-1	Upper Elkhorn #3/KY	HVA/Eastern	< 0.01
PSOC-154-1	Cannel/UT	HVC/Rocky Mountain	0.20
PSOC-188-1	Illinois #2/IL	HVB/Interior	0.96
PSOC-212-1	Ohio #2/OH	HVC/Eastern	0.01
PSOC-275-1	Upper Freeport/PA	Medium Volatile/Eastern	0.03
PSOC-309-1	New Mexico #8/NM	HVC/Rocky Mountain	0.06
PSOC-370-1	Hazard #7/KY	HVA/Eastern	0.02
PSOC-458-1	Blind Canyon/UT	HVA/Rocky Mountain	0.02
PSOC-483-1	Bed #53/WY	- /Rocky Mountain	0.02
PSOC-506-1	Upper Sunnyside/UT	HVA/Rocky Mountain	< 0.01
PSOC-538-1	Wadge/CO	HVC/Rocky Mountain	0.04

Note: Complete ASTM analyses for these specimens were reported in reference 3.

Sample source, Penn State University.

* Average of duplicate determinations.

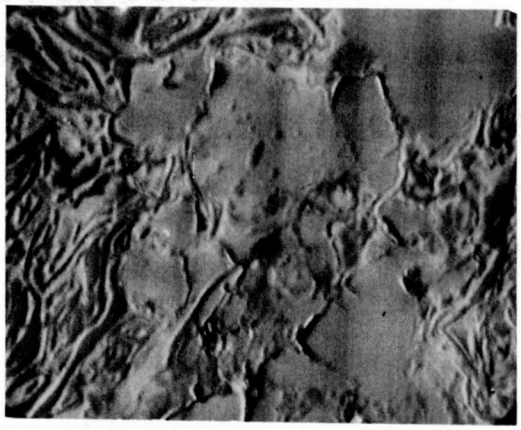

SPECIMEN CURRENT IMAGE

20 μm

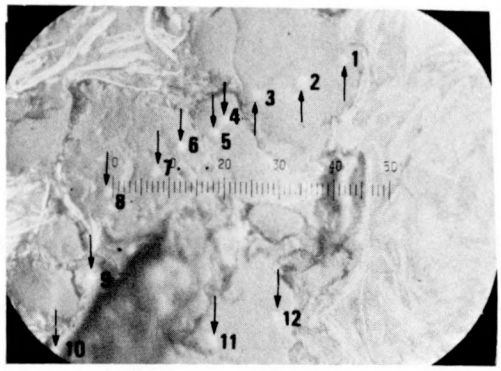

OPTICAL IMAGE

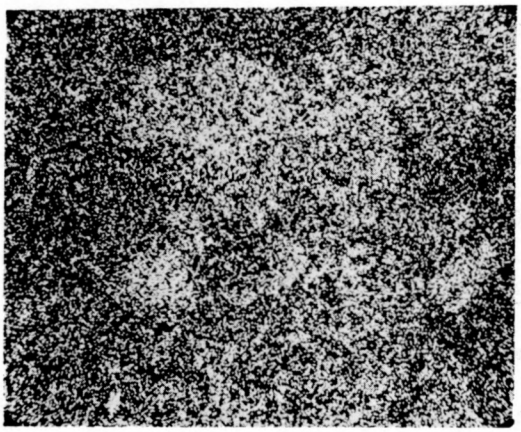

20 μm

SULFUR IMAGE

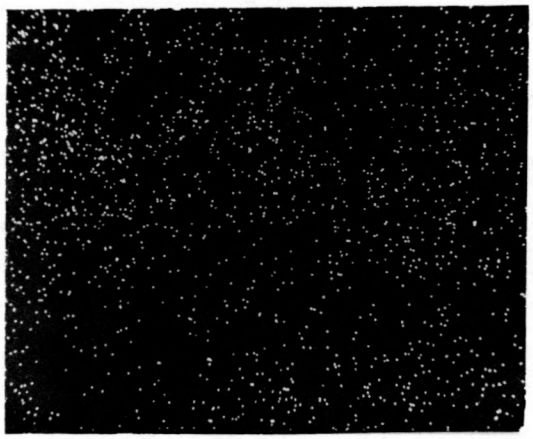

20 μm

No. 3637 COAL CONTROL SAMPLE (VITRINITE)

Figure 8. Organic sulfur point analyses on control coal sample number 3637. Vitrinite grains are probed with an electron beam (see contamination spots indicated by arrows in optical microscope image). A comparison of the specimen current image (showing the vitrinite grains) can be made with sulfur and with calcium distribution images. The sulfur distribution delineates the grain and appears uniform. No significant calcium patterns are seen (scan time = 3/4 hour; compare with Figure 9).

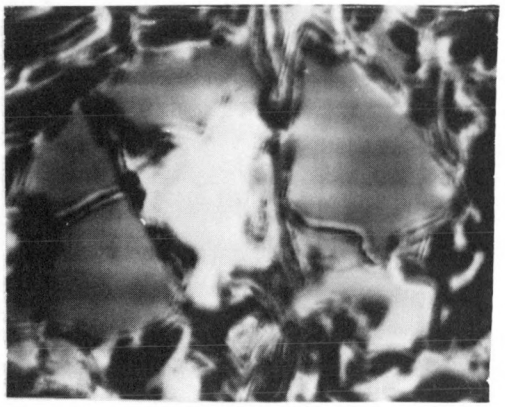

SPECIMEN CURRENT IMAGE 25 μm

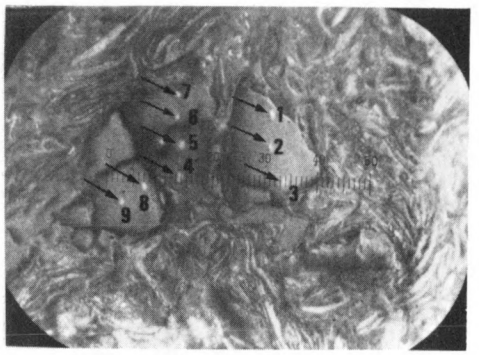

25 μm

OPTICAL IMAGE

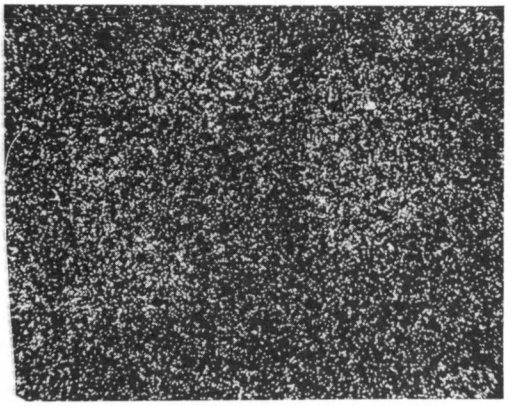

SULFUR IMAGE 25 μm

CALCIUM IMAGE 25 μm

No. 3718 DESULFURIZED COAL SAMPLE (VITRINITE)

Figure 9. Organic sulfur point analyses on desulfurized coal sample number 3718. Vitrinite grains are probed with an electron beam (see contamination spots indicated by arrows in optical microscope image). A comparison of the specimen current image (showing the vitrinite grains) can be made with sulfur and calcium distribution images. The sulfur distribution delineates the grains and appears uniform. Significant calcium patterns are seen in association with the vitrinite grains (scan time = 1/2 hour; compare with Figure 8). The desulfurization treatment possibly may release calcium from certain minerals into the leach solution, and quantities of this calcium may then be taken up by the macerals.

content of the vitrinite is <0.1 weight percent, whereas in the desulfurized examples, the calcium is ∿ 1 to 2 weight percent as was discussed in the preceding section.

B. Removal from Chemically Leached Coals

Initial studies have demonstrated the ability to quantitatively study the distribution of organic sulfur within a type of maceral. Additional data are being obtained prior to making any specific comments on the extent of the organic sulfur removal.

III. Other Activities

A. Elemental Sulfur Determinations

Fifteen well characterized coal samples have been provided by T. Squires for his exploratory studies of a new elemental sulfur determination technique based on CO_2 extraction. The results will be compared with available elemental sulfur determinations based on cyclohexane extractions of coal.

B. Chemical Leaching of Gypsum from Coal

Leached coal residues from the ASTM treatment for the determination of forms of sulfur in coal are being studied to determine if any significant amounts of inorganic sulfur remain in the residues. In this leaching process, coals are subjected to an HCl leach to remove sulfatic sulfur, and this is followed by an HNO_3 leach to remove pyritic sulfur. Jacobson and Benson (Ref. 1, page 10) report finding a mineral diffraction pattern in several of the residues that is very similar to gypsum ($CaSO_4 \cdot 2H_2O$). Evidence obtained in subsequent investigations establishes that the material is not gypsum.

Prior to the X-ray diffraction studies ASTM, sulfur determinations were completed. These results are reported in Table 4. To insure that no

significant oxidation of pyrite had occurred during the interval between the initial ASTM analysis and the period during which the X-ray work was performed, another set of ASTM analyses was performed on the same residues after the X-ray work on the residues was completed. As can be seen from the data in Table 5, no significant amounts of sulfatic sulfur were found. To check for possible encapsulation of gypsum which might prevent complete leaching of gypsum particles and thus result in low sulfatic values in Table 5, the residues were completely dissolved and analyzed by atomic absorption.

Table 5. Sulfatic Sulfur Deteminations of ASTM Leached Residues Subsequent to X-ray Studies.

Sample Number	Sulfatic Sulfur* weight % (DRY)
PSOC-003-1	0.07
PSOC-154-1	0.13
PSOC-188-1	0.19
PSOC-212-1	0.02
PSOC-275-1	0.09
PSOC-309-1	0.05
PSOC-370-1	0.12
PSOC-458-1	0.05
PSOC-483-1	0.05
PSOC-506-1	0.04
PSOC-538-1	0.07

*Average of duplicate determinations

Atomic absorption data for both calcium and barium are presented in Table 6. Calcium was determined so that possible levels of gypsum remaining in residues could be estimated. As the Ca levels are less than a few hundred µg/g, the amounts of gypsum remaining in residues for these samples is negligible. Barium was monitored to establish the presence of any barite ($BaSO_4$, an insoluble sulfate), in the residues; none was found (the specific minimum detection levels were below 13 µg/g Ba in all cases examined; Table 6).

Table 6. Atomic Absorption Measurements on Leached Coal Residues.

Sample Number	Calcium, µg/g	Barium, µg/g
PSOC-003-1	77	< 4
PSOC-154-1	232	< 9
PSOC-188-LA	155	< 13
PSOC-212-1	38	< 4
PSOC-275-1	127	< 4
PSOC-309-1	103	< 10
PSOC-370-1	70	< 7
PSOC-458-1	65	< 4
PSOC-483-1	42	< 9
PSOC-506-1	62	< 4
PSOC-538-1	22	< 5

Note: µg/g = microgram/gram

LITERATURE CITED

1. Greer, Raymond T., "Microstructure of Coal," in Quarterly Technical Progress Report, January 1, 1979 - March 31, 1979, IS-4703, prepared for DOE - Fossil Energy by Ames Laboratory, Iowa State University, Ames, Iowa, pp. 1-8, 1979.

2. Greer, Raymond T., "Microstructure of Coal," in Quarterly Technical Progress Report, October 1, 1978 - December 31, 1978, IS-4634, prepared for DOE - Fossil Energy by Ames Laboratory, Iowa State University, Ames Iowa, pp. 1-56, 1979.

3. Greer, Raymond T., "Characterization of Coal Microstructure," in Fossil Energy Annual Technical Progress Report, Advanced Development of Fine Coal Desulfurization and Recovery Technology, October 1, 1977 - September 30, 1978, IS-4668, Ames Laboratory, Iowa State University, Ames, pp. 58-61, 1979.

B. SELECTIVE MAGNETIC ENHANCEMENT OF PYRITE IN COAL BY DIELECTRIC HEATING

Delwyn D. Bluhm
Glenn Fanslow

Abstract:

The magnetic susceptibility of pyrite in coal is being enhanced by the use of selective pretreatments such as dielectric heating and chemical oxidation. Dielectric properties measurements of a selection of representative coals are being continued. Preliminary results indicated that several dielectric properties were inconsistent and should be measured again using a new sample. Measurements are being continued over a broad range of the frequency spectrum since there may be an optimum frequency where pyrite may be heated significantly faster than coal. Dielectric heating at 2.45 GHz was continued using a one-fourth height WR-340 slotted waveguide. Experiments on the parallel plate applicator that was developed for use at 27 MHz were performed to determine the impedance matching system. Dielectric heating of coal-derived pyrite at 2.45 GHz and 27 MHz is being performed to determine the parameters required to enhance the susceptibility and the reaction products produced by the pretreatments.

Objectives and Scope of Work:

The objective of this project is to improve the magnetic separation of coal and pyrite by enhancing the magnetic susceptibility of the pyrite in coal through the use of selective pretreatments of dielectric heating and chemical oxidation. The separation of pyrite from coal would be facilitated by altering a part of each pyrite particle to a more magnetic

form. Program projects include:

-- Measurements of dielectric properties of representative coals over a broad range of frequency spectrum for the identification of an optimum frequency where pyrite may be heated significantly faster than coal.

-- Experimental dielectric heating at 2.45 GHz and 27 MHz including alternate methods of continuous feed and experimental chemical oxidation of various coals.

-- The analysis and evaluation of the enhanced product accomplished by a number of techniques: ASTM analytical chemistry methods identifying the normal parameters of coal, x-ray diffraction methods for powders and single crystals, microprobe analyzer techniques, magnetic susceptibility measurements and mass spectrometer determination of the reaction products.

STATUS

Dielectric Properties Measurements - - Coal is a highly non-uniform material with contents that differ from mine to mine and even at points within a seam of coal, as shown by Greer (1). Therefore, it is necessary to recognize that the dielectric properties obtained for coal will also differ. However, to determine the degree of selective dielectric heating of pyrite in coal, it is essential to know typical values for the dielectric properties of these materials. Therefore, a selection of representative coals has been obtained and prepared for dielectric property measurements by Dr. S. O. Nelson of the USDA in Athens, Georgia (2).

The listing of the representative coals and the corresponding analysis

are shown in Table 1. Preliminary results suggest that, for the selective dielectric heating of coal in pyrite, it may be better to treat different coals at different frequencies. Additional work is being performed to check the initial measurements and to obtain a general profile of the dielectric properties to be found in coals.

I.D. No.	Material	Total Sulfur	Pyritic Sulfur	Ash	Moisture	BTU
02-21-043	DAHM R.O.M.	2.99	1.54	11.21	4.96	12,103
02-21-044	DAHM 1.30 Float	1.66	.30	3.26	10.67	13,180
02-21-045	DAHM 2.00 Sink	43.00	42.30	59.41	1.29	2,121
02-21-046	ILLINOIS #6 R O.M.	4.09	3.01	19.90	3.05	11,082
02-21-047	ILLINOIS #6 1.30 Float	1.82	.40	3.23	3.17	13,783
02-21-048	ILLINOIS #6 2.00 Sink	12.51	11.75	70.41	2.08	2,048
02-21-049	KENTUCKY #11 R.O.M.	3.26	.98	9.02	3.15	12,839
02-21-050	KENTUCKY #11 1.30 Float	2.69	.45	3.40	3.09	13,740
02-21-051	LIGNITE R.O.M.	1.49	.49	10.04	12.08	9,359
02-21-052	PITTSBURGH #8 R.O.M.	2.77	1.25	16.26	1.05	12,456
02-21-053	PITTSBURGH #8 1.30 Float	1.75	.17	4.31	0.92	14,526
03-21-054	PITTSBURGH #8 2.00 Sink	9.61	8.42	78.23	1.18	936

Table 1. Representative Coals for Dielectric Properties Measurements

Dielectric Heating - - Dielectric heating of pyrite in coal was investigated by heating mixtures of these materials at 2.45 GHz. Preliminary results were reported at the XIV International Microwave Power Symposium (3). It was shown that at 2.45 GHz, pyrite heated 2.6 times faster than coal as compared to a predicted value of 3.2.

Dielectric heating at 2.45 GHz is being continued using a one-fourth height WR-340 slotted waveguide. This provides a high electric field and

produces the most rapid reaction on the pyrite particles. A disadvantage is that sample size is limited and only small portions of treated product have been obtained. Alternate methods of continuous feed are being investigated. They include using a rotating tube, a vibrating glass plate and a drag cup transport mechanism. Recent work has been directed towards heating run-of-mine coals. Some of the problems encountered include the setting up of standing waves which cause hot spots to occur in the coal samples. The redesign of the experimental process which includes continuous feed is expected to eliminate this problem. Dielectric heating at 27 MHz is to be performed using a parallel plate applicator. However, before this can be accomplished, an impedance matching system had to be developed to match the impedance of the parallel plate, loaded with the coal or coal products, to the 50 ohm impedance of the 27 MHz source. This involved determination of typical impedances of the parallel plate with coal and pyrite and the determination of the values for the components required to match the source to these impedances. The Pi network shown in Figure 1 is to be used for this purpose.

It is to be noted that the capacitance of the parallel plate will be one branch of the Pi network. Representative values for X_L, R_L, Z_A, and Z_C are 65, 10,000, 4 and 55 ohms respectively. Parts for the matching network have been obtained and construction has begun.

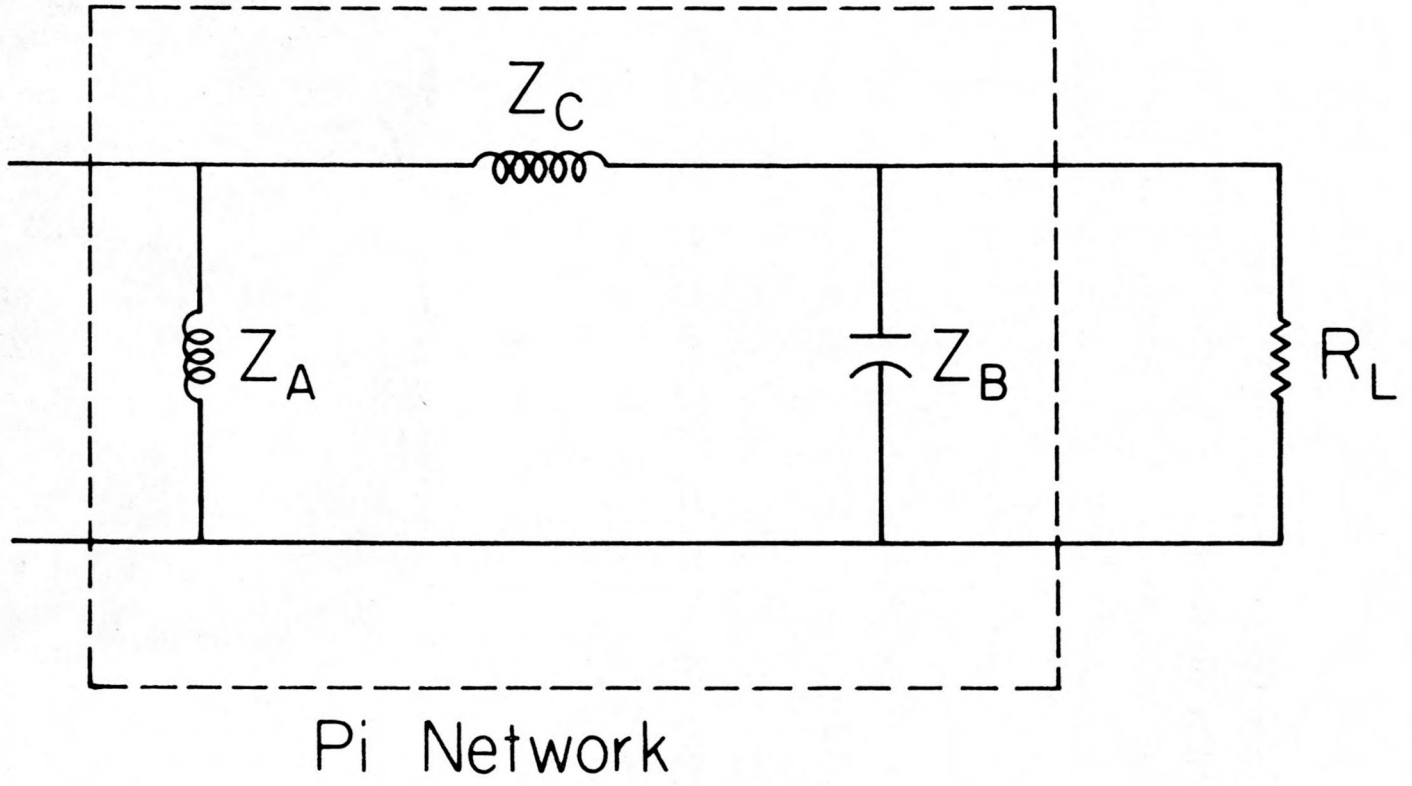

Figure 1. Pi Network for Matching the Parallel Plate Applicator in 27 MHz 50 ohm Source

Analysis and Evaluation of Enhanced Product - - The analysis and evaluation of the enhanced product is being accomplished by different techniques. ASTM analytical methods for identifying the normal constituents, x-ray diffraction methods for powders and single crystals, microprobe and analyzer techniques, magnetic susceptibility measurements and mass spectrometer analysis. The major work this period focused primarily on mass spectrometer analysis of the reaction products of microwave heated pyrite. Since chemical grade pyrite behaves quite differently under microwave heating, it is imperative that only coal-derived pyrite be used. Figure 2 is a photomicrograph of sample 02-21-005 of coal-derived pyrite heated dielectrically.

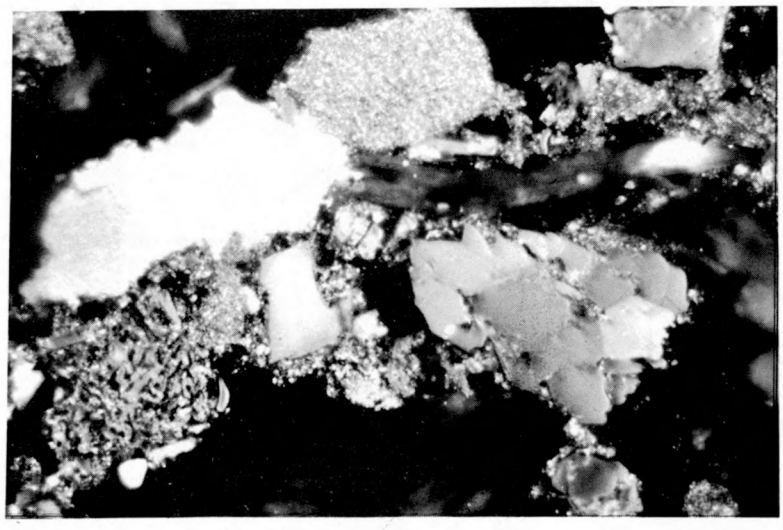

Figure 2. Photomicrograph of Sample 02-21-005 Coal-Derived Pyrite Heated Dielectrically

Observations of Figure 2 indicate that some pyrite is unaffected, some has been partially converted, and some has been totally converted to more magnetic forms of pyrite such as moniclinic pyrrhotite Fe_7S_8 (tentative identification). Precise identification of these materials is pending the results of microprobe analysis.

Analysis of the reaction products produced by dielectric heating of coal-derived pyrite is being obtained using a mass spectrometer. The method is to insert leached pyrite in a special sample holder, draw a vacuum on the sample and back fill it with oxygen. The sample is then heated at 2.45 GHz to a point where it has been shown that practically all of the material responds to a small permanent magnet. The reaction gases produced are then analyzed by a mass spectrometer. Initial results show that only minimal amounts of SO_2 are released. The most abundant gas was CO_2 with lesser amounts of COS, CS_2 and some hydrocarbons. This work is being continued with more rigid control of sample purity.

BIBLIOGRAPHY

1. Greer, R. T., "Pyrite Distribution in Coal", Scanning Electron Microscope Copy, 1978, Volume 1, SEM, ink., AMF.

2. Nelson, S. O., "Frequency Dependence of the Dielectric Properties of Wheat and the Rice Weevil", Ph. D. Dissertation, Iowa State University, Ames, Iowa, 1971. Publication #72-19997, University Microfilms, Ann Arbor, Michigan.

3. Fanslow, G. E., D. D. Bluhm and R. L. Simpson, "Dielectric Heating in Mixtures of Coal and Pyrite", Digest of XIV International Microwave Power Symposium, Monte Carlo, Monaco, June, 1979.

C. Rapid Analysis of Mineral Content of Coals: Development of an On-Line Monitoring Instrument for Pyrite and Ash in Coal.

J. E. Benson and R. A. Jacobson

Objective:

Our objective is to develop an easy-to-use instrument system for the rapid and accurate analysis of coal samples to obtain qualitative and quantitative information on the mineral content.

Progress:

Our first attempt to test the effects of a moving sample on the diffraction pattern of pyrite in coal was not successful due to a design error in the equipment we had built. This error has been corrected and the mechanical parts of the instrument have been reassembled.

To better understand the pyrite that occurs in coal, several single crystals of pyrite were chosen from different coal samples (ISU Mine #1, Mish Mine, and Dahm Mine - all in Iowa). Single crystal x-ray data were collected on four such crystals. Although the lattice constants of all four crystals indicated cubic symmetry, the single crystal data were collected as though the crystals were triclinic. There are sufficient violations of extinction conditions of the cubic space group $Pa\bar{3}$ and all other cubic space groups to indicate that the symmetry is indeed lower, either monoclinic or triclinic.

The reflections that we see that violate cubic, tetragonal and orthorhombic space groups are either too weak to be seen in a powder diffraction pattern or are marginally observed and occur at the same

diffraction angle in a powder pattern as a much stronger peak. In the four-octant data set of 1200 observed reflections, approximately 75-100 reflections are of the type that reduce the symmetry to monoclinic or triclinic.

We have refined the structure of our four pyrite crystals by putting the iron atoms in the same positions as they would occupy in the cubic structure and allowing the sulfur atom positions to vary. Although we get the conventional residual indices ($\Sigma||Fo|-|Fc||/\Sigma|Fo|$, where Fo is the observed structure factor, and Fc is the calculated structure factor, of 3.8% to 4.2% for the structures, the Fc's of the weak reflections are still in very poor agreement with the corresponding Fo's. A difference electron density calculation points to a partial disordering of the structure; the evidence is certainly not conclusive as yet.

We have undertaken this single crystal study for two reasons. First, we have observed that relative intensities of the powder diffraction lines that we obtain for coal derived pyrite does not match the relative intensities given in the JCPDS or ASTM files. By obtaining the intensities from a single crystal, it is possible to calculate a valid standard powder diffraction pattern. We have hand-calculated one such pattern, and are now in the process of writing a computer program to do this type of calculation routinely. The first calculated powder pattern fits our observed data very closely, and agrees well with work reported at the ACA meeting in Hawaii.[1]

This deviation from cubic symmetry for single crystal pyrite is also in accord with some recent optical microscopy studies in which weak but significant deviations from cubic symmetry were observed.[2] Diffraction

studies of this type could indeed be basic to a better understanding of the processes that take place in various treatments such as those designed to make "magnetic FeS_x species".

We have run one simple experiment to try to determine what the crystalline material is that we have observed in the coal residue following ASTM pyritic sulfur determination. A coal sample was boiled for one-half hour in HNO_3. This sample was washed according to the ASTM directions. Since water should not interfere with an x-ray powder diffraction analysis, the sample was examined while still wet. We did not observe any mineral pattern in the diffraction pattern other than quartz. The sample was allowed to air dry over a 48-hour period and the diffraction pattern was rerun. A new mineral pattern was then clearly visible in this air-dried sample. We have not identified this material as yet, nor are we even sure that it is a single species. We can readily identify two diffraction peaks from this material, but the presence of quartz in the sample causes difficulty in determining the exact diffraction angle of any more of the diffraction peaks.

We had planned at some time in the future to experiment with different wavelengths of x-rays to choose which wavelength would give the best combination of intensity of the mineral diffraction pattern and the least amount of overlap in the diffraction patterns from the more common minerals in coal. Since we were unfortunate enough to have our Mo tube burn out during this period, we have begun to make some measurements using Cu x-rays. The absorption of Cu x-ray radiation by iron bearing minerals completely eliminates the possibility of using this most popular of all x-ray sources for pyrite determination in coal. According to a Bureau of Mines publication, Ag is also eliminated[3] because this short wavelength (.56 Å)

causes severe overlap problems from kaolin, and we feel it would also cause an overlap problem with marcasite on the strongest diffraction line of pyrite.

Future Work:

Until we receive shipment of a new Mo x-ray tube (60 days) we will be forced to work on some of the other projects we have started, such as the pyrite structures, and the mineral that is being created and passed through the ASTM pyritic sulfur determination. We also will do some more experimental work on the determination of the rank of coal using x-ray diffraction. We will also try to separate or at least concentrate the different maceral types by float-sink techniques using organic liquids and a centrifuge. The purpose of this separation is to see if we can obtain diffraction patterns for each maceral type so that we could, by the use of computerized curve fitting techniques, get a good estimate of the amount of each maceral type in bulk coal samples.

Literature Cited

1. Smith, Steven T; Snyder, Robert L. and Brownell, W. E. Minimization of Preferred Orientation in Powders by Spray Drying. Abstracts of the ACA Spring, 1979.
2. Bayless, Peter; Crystal Structure Refinement of a Weakly Anisotropic Pyrite; American Mineralogist 62, 1168-1172, 1977.
3. Schehl, R. R. and Friedel, R. A.; Computerized System for Quantitative X-Ray Diffraction Analysis of Pyrite in Coal. Pittsburg Energy Research Center Technical Progress Report 71, 1973.

D. COAL BLENDING EXPERIMENTS

Donald L. Biggs

Objective:

The objective of this research is to determine the mineralogy and fusion properties of ash taken from various coals with a view toward establishing better criteria for forming blends of coals with the least potential for slagging and fouling and greatest energy release. Knowledge of the ash behavior correlated with the maceral content of the coals will permit prediction of ashing behavior of blends of coals without prolonged testing.

Status:

Ashing of coals from the Dahm and Decker mines in the raw and washed states is now completed and the low temperature ashes have been submitted for chemical analysis. X-ray powder diffraction patterns of the ashes and blends of ashes from the subject coals have been taken and are presently undergoing interpretation.

Microscopic analyses of the two subject coals have been completed and the results are appended to this report. The group maceral average for the two mines is shown in Table I.

Table I

Average Group Maceral Content for the Dahm and Decker Coals

Maceral	Dahm Coal	Decker Coal
Vitrinite	87.73%	91.34%
Inertinite	8.36	7.58
Exinite	0.89	2.95
Pyrite	0.97	0.19
	100.00	100.00

The Dahm coal is considered to be of high volatile C bituminous rank. As shown in these analyses, the pyrite content is lower than would be expected for such a coal in Iowa and lower than other analyses taken from bulk samples. The discrepancy is due to the fact that most of the pyrite at the locality where this bed was sampled occurs in large nodules which were excluded from the microscopic analysis. The exclusion of large pyrite bodies is justified on the grounds that it would be removed in the simplest sort of coal preparation. It is true that, at the Dahm Mine, a simple dry breaker treatment is used and most of the large nodules are removed in the process.

Comparison of the upper and lower halves of the Dahm seam show that the deposit is of rather uniform composition throughout its thickness. Slight variation is seen when the seam is divided into fourths and analyzed in that way. Except for the slight increase in inertinite and decrease in vitrinite in the second quartile, the deposit is almost uniform.

The Decker coal is considered to be of subbituminous rank. As such, much of the vitrinite is mixed with the precursor maceral, huminite. In some of the specimens huminite predominates over vitrinite. In these instances the vitrinite nomenclature is maintained, but the sample is marked by an asterisk indicating that some or all of the vitrinite is really huminite.

Comparison of the Decker coal by either halves or quarters shows that the lower portion of the coal is more vitrinitic than the upper part. The core from which the samples were taken did not reflect the upper ten feet of the deposit, and so the analysis may be somewhat distorted because of this missing information. Coals of this type disintegrate rapidly upon exposure to the atmosphere. This accounts for the fact that the core recovery was poor and the state of the core that was recovered being very difficult to make into adequate samples for microscopic observation.

APPENDIX I

Group Maceral Analysis of Decker Coal

	1A		1B		1C		1D		2A		2B	
V	6760	89.48	11875	89.69	14925	89.24	11425	88.74	9025	86.99	8950	89.95
I	265	3.51	975	7.36	675	4.04	950	7.38	600	5.78	700	7.04
E	465	6.15	275	2.08	975	5.83	425	3.30	675	6.51	175	1.76
P	65	.86	115	.87	150	.90	75	.58	75	.72	125	1.26
Σ	7555		13240		16725		12875		10375		9950	

	3A		3B		3C		3D		4A		4B	
V	3390	78.84	11435	83.56	18465	94.69	17470	92.77	7795	92.96	7090	80.11
I	575	13.37	1620	11.84	550	2.82	660	3.50	465	5.55	1125	12.71
E	275	6.40	335	2.45	410	2.10	545	2.90	125	1.49	635	7.18
P	66	1.40	295	2.16	75	.38	155	.82	0	0.00	0	---
Σ	4300		13685		19500		18830		8385		8850	

	4C		5		6A		6B		6C		6D	
V	9055	85.83	12100	90.64	10775	90.89	9435	88.72	14210	92.30	5450	86.71
I	1230	11.66	610	4.57	575	4.85	790	7.39	775	5.03	350	5.57
E	210	1.99	320	2.40	490	4.13	470	4.39	360	2.34	260	4.14
P	55	.52	320	2.40	15	0.13	0	0.00	50	0.32	225	3.58
Σ	10550		13350		11855		10695		15395		6285	

	6E		7A		7B		8		9A		9B	
V	8075	94.44	12540	86.51	3385	77.82	7825	86.94	11490	85.75	3000	68.18
I	325	3.80	1705	11.76	475	10.42	800	8.89	1575	11.75	1075	24.63
E	150	1.75	240	1.66	365	8.39	100	1.11	160	1.19	225	5.11
P	0	0.00	10	0.07	125	2.87	275	3.06	175	1.31	100	2.27
Σ	8550		14495		4350		9000		13400		4400	

	9C		10A		10B		10C		10D		11	
V	7480	84.52	6420	68.66	7810	85.50	7830	85.34	11510	90.99	13210	89.41
I	870	9.83	2225	23.80	800	8.76	745	8.12	590	4.66	885	5.99
E	405	4.58	690	7.38	515	5.64	385	4.20	525	4.15	475	3.21
Σ	8850		9350		9135		9175		12650		14775	

	12		13		14A		14B		15A		16A	
V	8800	77.02	7395	81.99	8090	85.38	8775	92.51	7150	88.27	6445	89.51
I	1325	11.60	1300	14.41	725	7.65	525	5.54	550	6.79	650	9.03
E	250	2.19	290	3.22	435	4.59	125	1.32	300	3.70	105	1.46
P	1050	9.19	35	0.39	225	2.37	60	0.63	100	1.23	0	0.00
Σ	11425		9020		9475		9485		8100		7200	

	16B		17		18A		18B		18C		18D	
V	8025	75.53	5615	89.77	9190	94.99	9045	96.17	9590	89.84	8630	91.08
I	2000	18.82	475	7.59	200	2.00	175	1.86	675	6.32	460	4.85
E	325	3.06	165	2.64	275	2.84	185	1.97	385	3.61	355	3.75
P	275	2.59	0	0.00	10	0.10	0	0.00	25	0.23	30	0.32
Σ	10625		6255		9675		9405		10675		9475	

	19A		19B		19C		20A		20B		21A	
V	3745	82.76	12650	82.68	8605	94.04	12920	84.31	9550	77.48	6045	85.74
I	600	13.26	2250	14.71	225	2.46	1625	10.60	2370	19.23	475	6.74
E	165	3.65	300	1.96	195	2.13	655	4.27	125	1.01	250	3.55
P	15	0.33	100	0.65	125	1.37	125	0.82	280	2.27	280	3.97
Σ	4524		15300		9150		15325		12325		7050	

	21B		22A		22B		23A		23B		24A	
V	9335	77.57	3975	96.95	13750	96.42	6650	92.36	7820	92.54	2100	91.30
I	2200	18.28	75	1.83	300	2.10	250	3.47	300	3.55	200	8.70
E	440	3.66	50	1.22	165	1.16	125	1.75	325	3.85	0	
P	60	0.50	0	0.00	45	0.32	175	2.43	5	0.06	0	
Σ	12035		4100		14260		7200		8450		2300	

	24B		25A		25B		26A		26B		27A	
V	16250	92.20	9325	85.75	5725	86.09	1975	88.77	11500	74.39	11620	90.22
I	650	3.69	1350	12.41	825	12.41	75	3.37	3700	23.93	775	6.02
E	725	4.11	200	1.84	100	1.51	125	5.62	175	1.13	465	3.61
P	0	0.00	0	0.00	0	0.00	50	2.25	85	0.55	20	0.16
Σ	17625		10875		6650		2225		15460		12880	

	27B		27C		28A		28B		28C		29B	
V	7780	92.23	11480	98.50	2025	73.64	12015	98.08	7620	91.75	6015	99.83
I	125	1.48	25	0.21	675	24.55	75	0.61	615	7.41	0	0.00
E	130	1.54	150	1.29	25	0.91	75	0.61	25	0.30	0	0.00
P	400	4.74	0	0.00	25	0.91	85	0.69	45	0.54	10	0.17
Σ	8435		11655		2750		12250		8305		6025	

	29C		29D		30A		30B		30C		31A	
V	9825	97.76	9400	96.91	9450	87.30	9715	96.14	11890	78.07	9275	90.44
I	75	0.75	175	1.80	1050	9.70	250	2.47	2500	16.41	800	7.80
E	125	1.24	125	1.29	275	2.54	140	1.39	650	4.27	100	0.98
P	25	0.25	0	0.00	50	0.46	0	0.00	190	1.25	80	0.78
Σ	10050		9700		10825		10105		15230		10255	

	31B		31C	
V	9250	81.03	3920	61.09
I	1975	17.30	1675	26.07
E	175	1.53	750	11.67
P	15	0.13	75	1.17
Σ	11415		6420	

DAHM MINE SAMPLES (74 samples)

Total Number of Microns = 752500
752505/4 = 188125

Averages by Fourths

1 (0-188125, samples 1A-6B)

V	167681	89.13
I	12173	6.47
E	6691	3.56
P	1580	0.84
Σ	188125	

2 (188126-376250, samples 6B-15A)

V	161158	85.67
I	17691	9.40
E	6303	3.35
P	2973	1.58
Σ	188125	

3 (376251-564375, samples 15A-24B)

V	165412	87.93
I	16032	8.52
E	5109	2.72
P	1572	0.84
Σ	188125	

4 (564376-752500, samples 24B-31C)

V	165904	88.19
I	16984	9.03
E	4082	2.17
P	1155	0.61
Σ	188125	

Averages by Halves

1st Half (0-376250 microns, samples 1A-15A)

V	328839	87.40
I	29864	7.94
E	12994	3.45
P	4553	1.21
Σ	376250	

2nd Half (376251-752500, samples 15A-31C)

V	331316	88.06
I	33016	8.78
E	9191	2.44
P	2727	0.72
Σ	376250	

Average of Dahm Coal Seam

(752500 microns, samples 1A-31C)

V	660155	87.73
I	62880	8.36
E	22185	2.95
P	7280	0.97
Σ	752500	100.01

Note: Sample 29A is missing. No satisfactory polish was obtained.

APPENDIX II

Group Maceral Analysis of Decker Coal

	1		2		4		5		6		7	
V	12535	76.85	17025	92.73	17795	95.85	7180	92.05	11995	82.07	17665	95.54
I	3725	22.84	1205	6.56	580	3.12	555	7.12	2585	17.69	550	2.97
E	50	0.31	130	0.71	190	1.02	65	0.83	35	0.24	275	1.49
P	0	0.00	0	0.00	0	0.00	0	0.00	0	0.00	0	0.00
Σ	16310		18360		18565		7800		14615		18490	

	8		9		10		11*		12		13	
V	5350	46.40	9850	92.92	18600	97.00	7150	75.14	6200	55.36	16245	88.29
I	6130	53.17	725	6.48	490	2.56	2340	24.59	5000	44.64	2050	11.14
E	50	0.43	25	0.24	85	0.44	25	0.26	0	0.00	105	0.57
P	0	0.00	0	0.00	0	0.00	0	0.00	0	0.00	0	0.00
Σ	11530		10600		19175		9515		11200		18400	

	14		15		16		17		18*		19	
V	16710	94.86	13390	84.75	17075	77.09	9990	46.63	7435	98.61	15710	96.62
I	800	4.54	2335	14.78	4950	22.35	11375	53.07	40	0.53	510	3.14
E	105	0.60	75	0.47	125	0.56	65	0.30	65	0.86	40	0.25
P	0	0.00	0	0.00	0	0.00	0	0.00	0	0.00	0	0.00
Σ	17615		15800		22150		21430		7540		16260	

*Predominantly Huminite

	20*		21*		22*		23*		24*		25*	
V	8660	91.90	12230	96.53	10765	82.81	17530	97.07	14135	89.21	9405	98.28
I	700	7.43	385	3.04	2225	17.21	475	2.63	1560	9.85	10	0.10
E	55	0.58	55	0.43	10	0.08	55	0.30	150	0.95	125	1.31
P	0	0.00	0	0.00	0	0.00	0	0.00	0	0.00	30	0.31
Σ	9415		12670		13000		18060		15845		9570	

	26*		27*		28*		29*		30*		31*	
V	17975	95.74	13700	99.17	9665	98.27	13430	94.61	8900	94.58	14955	92.60
I	0	0.00	30	0.22	80	0.81	60	0.42	315	3.35	785	4.86
E	600	3.20	30	0.22	15	0.15	60	0.42	50	0.53	105	0.65
P	0	0.00	55	0.40	75	0.76	645	4.54	145	1.54	305	1.89
Σ	18575		13815		9835		14195		9410		16150	

	32*		33		34*		35		36		37	
V	11250	87.24	14105	97.14	16765	97.16	16675	92.25	13560	95.53	15750	88.48
I	1510	11.71	305	2.10	340	1.97	1075	5.95	490	3.45	1600	8.99
E	75	0.58	100	0.69	150	0.87	275	1.52	85	0.60	450	2.53
P	60	0.47	10	0.07	0	0.00	50	0.28	60	0.42	0	0.00
Σ	12895		14520		17255		18075		14195		17800	

*Predominantly Huminite

	38		39		40*		41*		42		43	
V	9800	85.22	15050	91.35	9695	86.83	7645	72.88	10670	85.91	10775	96.42
I	1650	14.35	1075	6.53	1185	10.61	2785	26.55	1630	13.12	375	3.36
E	50	0.43	350	2.12	285	2.55	60	0.57	120	0.97	25	0.22
P	0	0.00	0	0.00	0	0.00	0	0.00	0	0.00	0	0.00
Σ	11500		16475		11165		10490		12420		11175	

	44		45		46		47		48*		49	
V	11260	98.04	12670	91.58	12570	99.49	11520	98.00	15925	100.00	12945	96.64
I	175	1.52	750	5.42	25	0.20	135	1.15	0	0.00	310	2.31
E	50	0.44	415	3.00	40	0.32	100	0.85	0	0.00	140	1.05
P	0	0.00	0	0.00	0	0.00	0	0.00	0	0.00	0	0.00
Σ	11485		13835		12635		11755		15925		13395	

	50		51		52*		53*		54		55*	
V	11940	98.68	11475	100.00	17550	100.00	13560	99.71	9485	98.29	13220	94.77
I	35	0.29	0	0.00	0	0.00	0	0.00	150	1.55	180	1.29
E	125	1.03	0	0.00	0	0.00	40	0.29	15	0.16	50	3.94
P	0	0.00	0	0.00	0	0.00	0	0.00	0	0.00	0	0.00
Σ	12100		11475		17550		13600		9650		13950	

*Predominantly Huminite

	56		57		58		59		60		61*	
V	13635	99.16	14670	99.59	14115	98.57	13645	99.02	9540	98.45	13150	96.90
I	35	0.25	10	0.07	100	0.70	25	0.18	75	0.77	75	0.55
E	80	0.58	50	0.34	105	0.73	110	0.80	75	0.77	220	1.62
P	0	0.00	0	0.00	0	0.00	0	0.00	0	0.00	125	0.92
Σ	13750		14730		14320		13780		9690		13570	

	62		63*		64		65*		66*		67	
V	11800	98.13	15055	96.66	15615	97.20	17080	98.05	11900	94.44	13365	92.68
I	30	0.25	450	2.89	310	1.93	125	0.72	620	4.92	250	1.73
E	195	1.62	70	0.45	140	0.87	215	1.23	80	0.63	600	4.16
P	0	0.00	0	0.00	0	0.00	0	0.00	0	0.00	205	1.42
Σ	12025		15575		16065		17420		12600		14420	

11B* (two samples were taken)

V	5225	100.00
I	0	0.00
E	0	0.00
P	0	0.00
Σ	5225	

*Predominantly Huminite

DECKER MINE SAMPLES (67 samples)

Total Number of Microns = 929160
929165/4 = 232290

Averages by Fourths

1 (0-232290, samples 1-17)

V	195774.50	84.28
I	35169.00	15.14
E	1346.50	0.58
P	0.00	0.00
Σ	232290.00	100.00

2 (232991-464580, samples 17-34)

V	210064.43	90.43
I	19241.02	8.28
E	1659.55	0.71
P	1325,00	0.57
Σ	232290.00	99.99

3 (464581-696870, samples 34-51)

V	215861.07	92.93
I	13609.98	5.86
E	2708.95	1.17
P	110.00	0.05
Σ	232290.00	100.01

4 (696871-929160, samples 51-67)

V	226980.00	97.71
I	2435.00	1.05
E	2545.00	1.10
P	330.00	0.14
Σ	232290.00	100.00

Averages by Halves

1st Half (0-464580, samples 1-34)

V	405838.93	87.36
I	54410.02	11.71
E	3006.05	0.65
P	1325.00	0.29
Σ	464580.00	100.01

2nd Half (464581-929160, samples 34-67)

V	442841.07	95.32
I	16044.98	3.45
E	5253.95	1.13
P	440.00	0.09
Σ	464580.00	99.99

Average of Decker Coal Seam

(929160 microns, samples 1-67)

V	848680	91.34
I	70455	7.58
E	8260	0.89
P	1765	0.19
Σ	929160	100.00

II. Advanced Research and Technology

A. DIRECT UTILIZATION- RECOVERY OF MINERALS FROM COAL FLY ASH

G. Burnet and M. Murtha

Abstract:

Developmental research of the chlorination and sintering processes for recovery of minerals from coal fly ash was continued. For the high-temperature gas chlorination (HiChlor) process a gas chromatograph was connected at the reactor exit. Samples of the noncondensible gases were analyzed at three minute intervals to measure the changes in rates of reactions during the chlorination run. Low temperature, 500 to 700°C, chlorination of fly ashes and of oxide mixtures shows that iron oxide is much more reactive than alumina at these temperatures and hence can be removed preferentially.

Investigation of the lime-soda sinter process revealed that the sintering reactions occur by solid phase diffusion of the reacting oxides. For mixtures of lime, silica, and alumina, homogeneous products resulted after sintering for two hours at 1,350°C. Further investigations show that CaO and SiO_2 reactions occur at lower temperatures and more rapidly than the CaO and Al_2O_3 reactions. This information is important to the design and operation of the lime-soda sinter process calciner.

Fly ash magnetic separation tests using a range of electromagnet power settings show that with increased power the mass of the magnetic fraction increases but the average iron content in this fraction decreases. The optimum iron separation occurs at power settings of 60 to 70 percent of full power.

Nonmagnetic fraction fly ash samples were divided into size fractions by a settling technique. Results of the analyses of these fractions indicate that the alumina concentration is highest in the small size fractions; silica and iron oxide concentrations are more independent of size. Design and operation of the chlorination reactor in the HiChlor process will be influenced by these results.

Background:

The primary objective of this investigation is to develop and/or improve methods for the utilization of coal fly ash as a source of minerals. Processes are being studied for the recovery of alumina, iron oxides, and titanium oxides from fly ash and for utilization of the residue. Use of fly ash as a source of

minerals will help the United States reduce its ash disposal problems and dependency upon imported ores and metals.

Objectives:

Task A - Development of HiChlor Process - Fly ash will react at about 800°C with chlorine gas in the presence of carbon as a reducing agent to form volatile metal chlorides. The chlorides can be condensed and separated to give the products desired. Details of the process remain to be developed, including an understanding of the reaction mechanism, a continuous fluidized bed reactor, a scheme for recycling excess reactants, and a method for recovering and separating the products.

Task B - Improvement of the Lime-Soda Sinter Process - Soluble sodium and calcium aluminates are formed when fly ash is mixed with the proper amount of limestone and soda ash and sintered at about 1100°C. The aluminates can be extracted from the clinker using a dilute soda ash solution. A commercial grade hydrate of alumina is recovered from the extract by precipitation. The sintering step is now well understood and work has been started on the remainder of the process. A proposal for construction and operation of a process development unit (PDU) as the first step toward commercialization of the process has been submitted for funding approval.

Task C - Recovery of an Iron-Rich Fraction from Fly Ash by Magnetic Separation- The above processes for metal recovery are improved by the removal of as much iron as possible from the feed mixtures. Bituminous coal fly ashes contain an average of about 18% iron oxides, a significant portion of which can be separated magnetically. The magnetic fraction consists of high-density, finely-divided, spheroidal particles, which can be used as heavy media material for coal and ore beneficiation. The amount of iron rich material available exceeds the demand for heavy media applications so its purity must be increased to where it can be used as an iron ore. Another coal waste containing significant quantities of iron is the refuse from coal washing plants. After coal refuse is ashed, the residue is similar in composition to magnetically separated, iron-rich coal fly ash.

Status:

HiChlor Process Development

1. Reaction Kinetics - To enable better understanding of the reactions occur-

ing when mixtures of coal fly ash and carbon are chlorinated, a gas chromatograph has been installed to measure the composition of the noncondensible gases. The condensible products such as $FeCl_3$, $AlCl_3$, and $TiCl_4$ are removed from the effluent gases by a cold trap, then the carbon oxides and excess chlorine compositions are determined by the gas chromatograph. A single chromatograph column maintained at 0°C separates CO, CO_2, and Cl_2 and permits sampling at about 5 minute intervals. These analyses at short intervals allow the reactions to be followed closely, detecting changes in reaction product formation rates and monitoring excess chlorine flow. Although $SiCl_4$ is not detected by the chromatograph column, the volume of $SiCl_4$ in each gas sample can be determined by difference because of the constant volume of the sample loop.

Replicate chlorination runs were made at 750, 800, and 850°C reaction temperatures. The results indicate that the CO and CO_2 volumes generated vary significantly with temperature.

2. Preferential Chlorination of Metal Oxides - Preferential chlorination of iron and aluminum oxides as a function of reaction temperature was investigated to determine the potential of pretreatment of the ash for the HiChlor fly ash chlorination process. The chlorination reactivity of pure oxides of iron and aluminum, and of mixtures of the two oxides was determined for the temperature range 500 to 700°C. The results were compared to chlorination data obtained earlier for fly ash.

It was found that chlorine reacts primarily with iron oxide at these relatively low temperatures. At a reaction temperature of 700°C, seventy to eighty percent of the iron oxides are chlorinated for both the pure oxides and the fly ash. Less than twenty percent of the aluminum oxide reacted in the pure compound tests. The reactivity of the alumina in the fly ash was even lower with only four percent being chlorinated. This indicates that lower temperature preferential iron chlorination may be used to separate most of the iron prior to alumina chlorination at a higher temperature.

3. Fluidization studies - Experiments continued on the determination of fluidization characteristics of coal fly ashes and of fly ash-charcoal mixtures. The effects of charcoal particle size and bed aspect ratio (bed height to diameter) on fluidization were examined. Also, several batches of fly ash and charcoal material were chlorinated to prepare a sample of sufficient quantity for investigation of the fluidization characteristics of partially

chlorinated fly ash.

The fluidization work was extended to include a subbituminous western coal fly ash. This material has a small mean particle diameter of about 12μ m and is cohesive and difficult to fluidize. Poor fluidization was observed because the fly ash tended to agglomerate to form larger particles, which inhibit the air flow and cause channeling through the bed.

Fluidization properties of fly ashes improve when charcoal is added. Charcoal and fly ash mixtures in a weight ratio of 3 to 10 were used, and the effect of charcoal particle size on fluidization was studied. Mechanical stirring was required as an assist to the gas flow to provide fluidization of new mixtures, but once the material had been fluidized a bed could be refluidized without stirring.

Fluidization of a mixture of fly ash and 53 to 147 μm size charcoal gave an appearance of good fluidization. However, the bed pressure drop data indicated that significant particle size segregation was occurring. Charcoal-fly ash mixtures for all the charcoal sizes used fluidized at the higher air flow rates used. Mixtures containing a wide range of charcoal particle sizes seemed to have the best fluidization characteristics, and the mixture with the smallest charcoal particles showed the poorest fluidization.

A series of experiments with mixtures of fly ash and 45 to 74 μ m diameter charcoal was made that included different bed depths. All of the beds fluidized well at air velocities greater than 0.4 cm/sec. Deeper beds do not appear to effect fluidization.

Overall, the results obtained to date suggest that fly ash-charcoal mixtures that would be used in a continuous fluidized bed chlorination reactor can be adequately fluidized.

Lime-Soda Sinter Process Improvements

1. Reaction Mechanism and Kinetics - A series of sintering runs at 1250°C and 1350°C were completed. The runs made at 1350°C showed evidence of liquid phase formation. This liquid forms amorphous material on cooling and amorphous material makes it difficult to interpret the results of x-ray diffraction analysis of these powders.

Samples were leached in a solution of maleic acid and methanol which dissolves calcium orthosilicate. The extracted residues were then analyzed by x-ray diffraction and with the removal of a major compound, the calcium orthosilicate, the peaks of the calcium aluminate compounds were easily identified.

These data showed that at 1250°C a sintering time of two hours is required for complete reaction of the lime.

The sinter products were also examined by electron microprobe (EM) to study the elemental distribution within the samples. These data indicate that the reactions are not complete after a 1 hour sinter at 1350°C. The product was found to be more completely reacted after a 2 hour sinter at 1350°C. The data in Figure 1, for a step scan of 2 μm/step across a sample, shows an area of unreacted alumina for a sample sintered for only one hour. After two hours it was difficult to find an area containing unreacted material, and any unreacted areas were small, indicating the progress of the reaction with time.

High temperature x-ray measurements were also made. This technique permits the detection of the transformation of solids and the formation of new compounds. The conclusions reached based on these measurements are as follows:

1. The reaction between CaO (C) and SiO_2 (S) begins at a lower temperature and finishes earlier when compared to the reaction between CaO (C) and Al_2O_3 (A).
2. In the ternary mixture of CaO, SiO_2 and Al_2O_3, reactions proceed as for mixtures of two binary systems, i.e., no ternary compounds were found.
3. For the reaction of CaO and Al_2O_3, CA and $C_{12}A_7$ form at first. The $C_{12}A_7$ disappears at 1000°C and C_3A and C_2A begin to appear. The formation of CA_6 is possible; however, it will form in very small amounts and exist for only a short time.

2. Limestone-Fly Ash Sinter Process - Sintering runs with mixtures of limestone and fly ash, plus additives, were made. Data on alumina solubilization were collected for sinters with the mineralizer CaF_2 added to the mixture. The alumina solubilization increased from 49.8 percent for the mix without CaF_2 to 72.7 percent when 20 weight percent CaF_2 was added. The addition of the mineralizer reduced the optimum sintering temperature from 1380°C to 1100°C.

Limestone-fly ash sinter runs were also made with pulverized coal refuse added to the mixture. It was postulated from other publications that coal refuse could be an effective reducing material. Previously testing with carbon and coal added shows no improvement in alumina solubilization but this time the addition of 5 weight percent coal refuse to the sinters resulted in an alumina solubilization of 66.5 percent. This is a significant increase

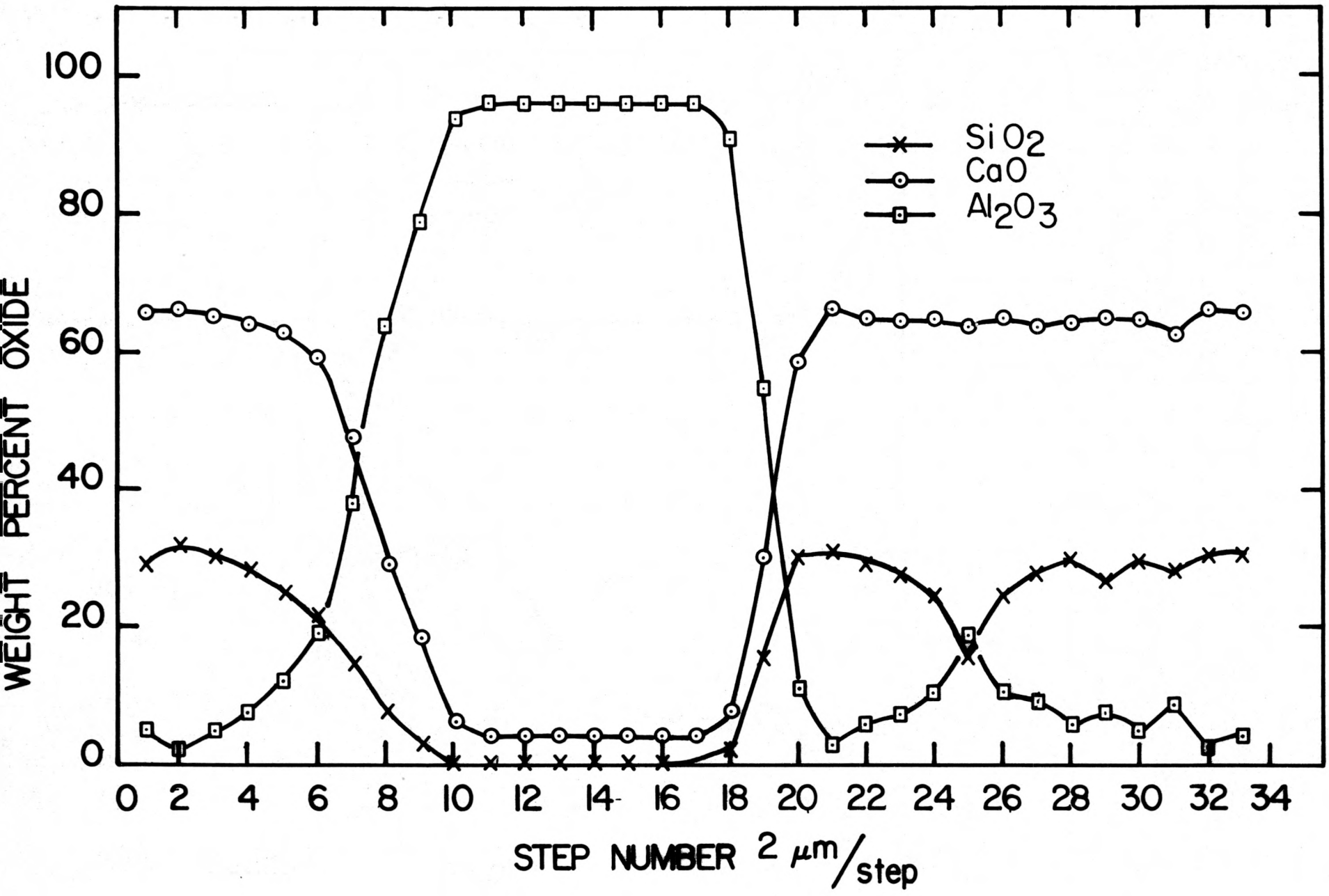

Figure 1. Radial distribution of oxides after sintering for one hour at 1350°C, measured by electron microprobe (EM).

above the 45 percent alumina solubilization obtained for this sinter composition without coal refuse added. These runs were made at 1380°C and additional investigation is planned.

3. Lime-Soda Sinter Research - Research with alternate limestone resources, with a range of sintering times, and an investigation of the desilication and the carbonation process steps is being conducted to provide information required for the design of an Ames Lime-Soda Process Demonstration Unit (PDU). A proposal for a PDU, processing 500 lbs. of fly ash per 8 hr.day, has been submitted to the Fossil Energy Division of USDOE.

Additional information on the above mentioned process steps is required for correct design and sizing of these items of process equipment. The time required for sintering will determine the size of the rotary kiln for a given throughput rate. The time and conditions for desilication will determine the capacity and pressure rating of the desilication vessel. Tests of the filtrate carbonation step will determine the degree of precipitation of dissolved constituents relative to one another as the pH of the solution decreases.

Tables 1 and 2 contain data on the sintering step and on the carbonation step, respectively. These results for five dissolved constituents were determined using the atomic absorption spectrophotometer. From Table 1, we see that partial precipitation will not provide a silica-free product. Therefore, it will be necessary to desilicate the filtrate before carbonation. Table 2 shows a slight reduction in alumina extraction from sinters as the sintering time is reduced from 60 minutes , to 30 minutes, to 18 minutes; but a sintering time of less than one hour does not appear to form the necessary insoluble calcium silicates, as indicated by the increased calcium and silica concentrations for the shorter runs. When filtrate desilications were conducted at 90 to 95°C, both the silica and the alumina precipitated. Research by the Bureau of Mines shows that a pressure of at least 200 psi is required for desilication of aluminate solutions without excessive alumina losses. Modifications are being made to the Parr pressure vessel so it can be used for small volume pressure desilication studies.

Table 1. Effect of pH on the Solubility of Constituents in Filtrate from Extraction*

Filtrate pH	PPM of Dissolved Element Al	Si	Fe	Ca	Ti
12.5	4900	44	1.1	0.1	0.2
11.0	2400	9	0.1	--	0.2
10.0	190	2	0.4	--	--
9.0	50	4	0.2	--	--

* pH reduced by bubbling carbon dioxide into filtrate

Table 2. Effect of Sintering Time on the Solubility of Constituents in Filtrate from Extraction

Sintering Time Min. at 1200°C	PPM of Dissolved Element in Filtrate Al	Si	Fe	Ca	Ti
1st set of runs					
60	4900	36	0.9	0.1	0.2
30	5000	44	0.6	0.9	0.2
18	4750	49	0.8	2.4	0.3
2nd set of runs					
60	4850	39	1.2	0.1	
30	4550	56	1.5	1.9	
18	4450	70	2.2	2.8	

Table 3. Compositions of Magnetic Fly Ash Fraction as a Function of Electromagnetic Separator Power.*

Power Setting % Rheostat	Wt. % Total Ash in Mag. Fraction	Wt% in Magnetic Fraction			% of Total Fe in Magn.Frac
		Fe_2O_3	SiO_2	Al_2O_3	
25	0.2	69.5	16.8	7.9	0.6
30	8.1	65.5	19.0	8.6	21.0
50	20.0	61.0	21.5	9.3	48.8
70	27.5	56.4	24.4	10.5	62.9
90	28.0	53.3	27.1	10.9	59.9
100	30.7	51.4	28.5	11.5	63.0

* Tests on a high-iron content Missouri Coal fly ash from the Montrose power station, La Due, Missouri operated by Kansas City Power and Light Company. Ash was collected using electrostatic precipitation.

Recovery and Beneficiation of the Iron Rich- Fraction of Coal Fly Ash

Tests were conducted to determine the effect of electromagnetic separator power setting on the separation of fly ash. A high-iron-content Missouri coal fly ash was used, and the magnetic ash fraction was separated, weighed, and analyzed for six power settings. These data, shown on Table 3, indicate that, with increasing power to the magnet, the magnetic fraction contains progressively higher concentrations of silica and alumina. The maximum amount of iron recoverable from this fly ash by magnetic separation is about 60 percent and this fraction is most concentrated at a power setting of 70 percent. There is no benefit to using higher power settings for magnetic fly ash recovery with this electromagnetic separator.

Some preliminary work has been done to determine the possibility of demagnetizing the residual magnetism in the magnetic ash. A roasting method was tested using the Missouri ash magnetic fraction. Figures 2 and 3 show photographs in water suspensions of dispersions of Missouri magnetic ash before and after roasting at 600°C for 1 hour. These results indicate that roasting may destroy residual magnetism.

Other possible methods, physical as well as chemical, on beneficiation of the iron-rich fraction are being conducted. A sample has been sent to the Sturtevant Mill Company for ultra fine grinding. Fine grinding of the magnetic ash may liberate the impurity particles from the magnetic particles. Further processing, floatation or magnetic separation, may then separate the impurities to give a beneficiated iron product.

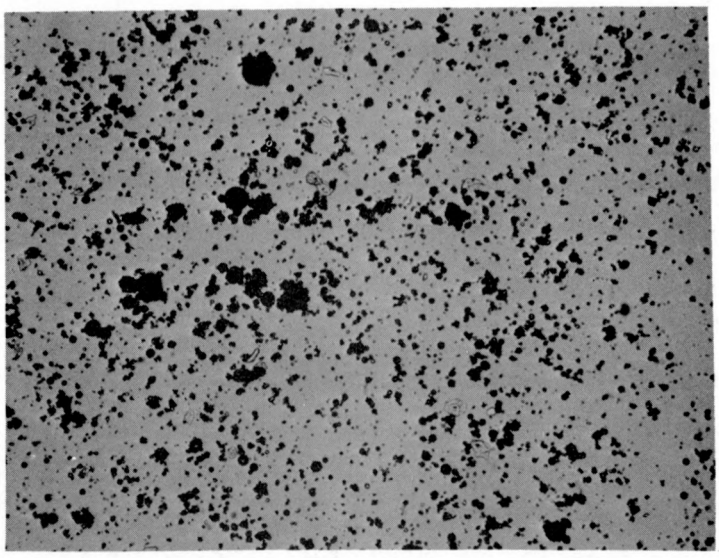

Figure 2. Magnetic Fraction of Missouri fly ash as separated, dispersed in water (280X).

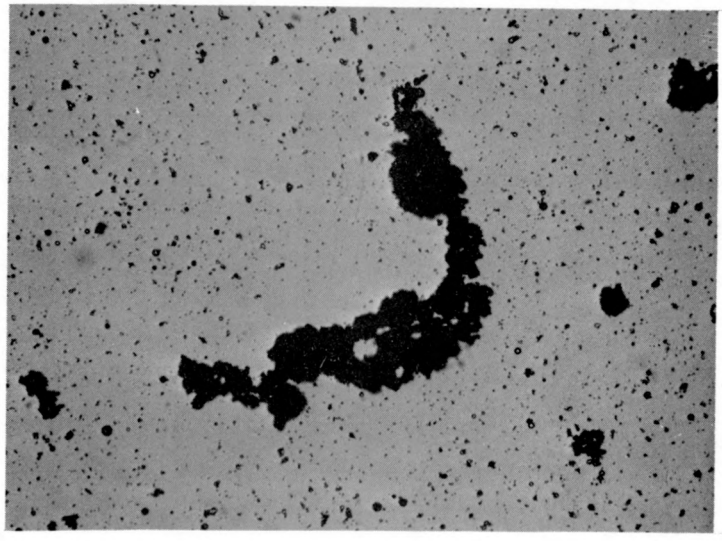

Figure 3. Magnetic Fraction of Missouri fly ash roasted for one hour at 600°C dispersed in water (280X).

Table 4. Summary of Data For Size-Fractionated Nonmagnetic Portions of Fly Ash.

Coal Fly Ash	Size Fraction, μm*		Wt. % Total Ash	Composition, Oxide wt. %			
	Calculated Range	Measured Mean	in Nonmag. Fraction	SiO_2	Al_2O_3	Fe_2O_3	CaO
Missouri**	+ 63		6.67	54	12	9	13
	31-63	25	13.76	57	12	14	13
	18-31	20	47.34	56	17	10	8
	11-18	10	9.09	52	21	10	4
	1-11	4	23.14	52	22	10	3
		Total	100.00				
Kentucky***	+ 63		6.60	40	11	30	8
	31-63	22	16.32	39	14	34	8
	18-31	17	22.73	50	16	15	9
	11-18	15	25.73	52	19	12	6
	1-11	4	28.62	53	21	10	4
		Total	100.00				

*The size fractions were separated into calculated size ranges by a settling procedure. The fractions were then analyzed for size distribution using the Coulter counter. The particle diameters measured were smaller than the sizes calculated by settling possibly because of agglomeration of small particles or because of the presence of higher density particles.

** See Table 3 for identification of this fly ash.

*** A high-iron ash from a Kentucky coal burned at the Louisville Power Station. Ash recovered by electrostatic precipitation.

Investigation of the Substructure of Coal Fly Ash

Two nonmagnetic fractions of fly ashes from midwestern bituminous coals were each separated into five size fractions by a specially developed settling technique. These separated fractions were then chemically analyzed and the actual size distribution of each was determined by Coulter counter measurement.

Before the ash samples could be separated by settling it was necessary to find a method to prevent particle agglomeration since both nonmagnetic ashes tended to coagulate in water. By trial and error it was found that a sodium oxalate solution prevented coagulation. This type of anti-coagulant, an electrolytic peptizer, is thought to surround each particle with a like charged barrier. A sodium oxalate solution of less than one weight percent was found to prevent coagulation for over 12 hours. This solution was then used for the settling separations. The data on weight percent of each size fraction and chemical analysis of the individual fractions are given in Table 4.

The size determinations as measured by the Coulter counter show that the coarser fractions of both ashes consist of particles of smaller diameter than determined by settling. This discrepancy may be caused by the presence of a large number of small particles with densities higher than the average of the whole nonmagnetic ash fraction. It appears that Kentucky ash contains a higher number of high density particles than the Missouri ash.

The alumina and calium contents of the Missouri coal fly ash vary inversely with the size fractions. Alumina is highest in the finest size fraction and lime highest in the coarse fractions. The silica and iron oxide contents are more independent of particle size. In the case of the Kentucky coal nonmagnetic fly ash, the trends are the same except the iron oxide contents are high in the two coarse fractions and the silica level decreases somewhat for the two coarse fractions.

X-ray analysee of the Missouri ash fractions show that all fractions contain a major amount of SiO_2 in the form of quartz. Major intensity peaks of magnetite and hematite are found in the three coarses fractions. Another mineral identified is lime (CaO).

Microscopic particle observations reveal that many of the nonmagnetic particles have beads of magnetic material imbedded within them. Even with full magnetic power the magnetic force was insufficient to lift some of these

magnetic particles having an attached nonmagnetic mass. At higher magnetic strengths, a larger mass of nonmagnetic material can be lifted, however, and at the higher power settings the magnetic fraction should be of lower Fe_2O_3 content. This is confirmed by the data in Table 3.

The results in this section of the report provide information about ash composition that is important in the design of experiments to determine how the fly ash reacts in both the lime-soda sinter and HiChlor processes.

Future Work:

HiChlor Process Development

A vertical, downflow fixed-bed reactor will be connected directly to a gas chromatograph and chlorinations will be conducted with large chlorine excess to provide data required for the determination of the chlorination mechanism and of the reaction kinetics. Preferential chlorination as a method of beneficiation of fly ash will be continued using moderate reaction temperatures without carbon present.

Fluidization properties of chlorinated fly ash residues will be examined. Factors which may influence the fluidization characteristics will be verified using size analyses of entrained material as measured by the Coulter counter and using photo micrographs of bed material after fluidization. An investigation of the fluidization of mixtures of charcoal and other fly ashes and or mixtures of fly ashes and pulverized coal will be conducted.

Lime-Soda Sinter Process Development

Research will continue on the fundamental studies of the reaction mechanism of sintering reactions, using differential thermal analysis (DTA) and X-ray diffraction measurements. Different fly ashes will be treated by the lime-soda sinter method, and investigation of the precipitation and purification steps of the process will be expanded to include leaf filter tests on the extraction residue. High pressure desilication experiments for silica removal from extraction filtrates will be performed for a range of pressures and rates of lime addition. Investigation of the extraction and filtration steps of the lime-soda sinter process will be conducted as continuous rather than batch processes. The work will include verification of stirred tank extractor design calculations.

Recovery and Beneficiation of the Iron Rich Ash Fraction

Evaluation studies will continue on beneficiation methods, physical and chemical, for producing a low-alumina, low-silica product for use in the steel industry. A microground magnetic ash sample will be subjected to further magnetic separation and/or flotation separation in an effort to reduce silica and alumina impurity levels.

Experimental data will be collected on high-pressure caustic leaching of magnetic fly ash samples. The processing conditions which will be evaluated are NaOH concentration, temperature of extraction, and the ratio of NaOH to silica and alumina. Untreated magnetic ash, magnetic ash previously soaked in caustic solution as a pretreatment, and the microground magnetic fly ash will be pressure-leached.

Fly Ash Substructure

Separated fractions of the nonmagnetic coal fly ashes studied will be used for x-ray diffraction and microscopic observation to further identify substructure patterns in ash particles. Individual particles of the nonmagnetic ashes will be identified with respect to mineralogy, composition, and structure in an effort to classify ashes by particle substructure characteristics.

Distribution List

USDOE - CORO	1
USDOE - TIC	234
USDOE - Washington	30
Raymond Greer	20
Robert Jacobson	20
Donald Biggs	20
Ray Fisher	20
Delwyn Bluhm	20
George Burnet	20
Ames Laboratory Library	15
Total	405